Implementation of the ISORROPIA-lite Aerosol Thermodynamics Model into the EMAC Chemistry Climate Model 2.56: Implications for Aerosol Composition and Acidity

5   Alexandros Milousis[1], Alexandra P. Tsimpidi[1], Holger Tost[2], Spyros N. Pandis[3,4], Athanasios Nenes[3,5], Astrid Kiendler-Scharr[1+], and Vlassis A. Karydis[1]

[1]Forschungszentrum Jülich GmbH, Institute for Energy and Climate Research, IEK-8 Troposphere, Jülich, Germany
[2]Johannes Gutenberg University Mainz, Institute of Atmospheric Physics, Mainz, Germany
[3] FORTH ICE HT, Institute of Chemical Engineering Sciences, Patras 26504, Greece
10 [4]University of Patras, Department of Chemical Engineering, Patras 26500, Greece
[5]Ecole Polytechnique Fed Lausanne, School of Architecture Civil & Environmental Engineering Lab, Atmospheric Processes & Their Impacts, CH-1015 Lausanne, Switzerland
[+]deceased

15 *Correspondence to*: Vlassis A. Karydis (v.karydis@fz-juelich.de)

Abstract. This study explores the differences in performance and results by various versions of the ISORROPIA thermodynamic module implemented within the global atmospheric chemistry model EMAC. Three different versions of the module were used, ISORROPIA II v1, ISORROPIA II v2.3, and ISORROPIA-lite. First, ISORROPIA II v2.3 replaced ISORROPIA II v1 in EMAC to improve pH
20 predictions close to neutral conditions. The newly developed ISORROPIA-lite has been added to EMAC alongside ISORROPIA II v2.3. ISORROPIA-lite is more computationally efficient and assumes that atmospheric aerosols exist always as supersaturated aqueous (metastable) solutions while ISORROPIA II includes the option to allow the formation of solid salts at low RH conditions (stable state). The predictions of EMAC by employing all three aerosol thermodynamic models were compared to each other and
25 evaluated against surface measurements from three regional observational networks (IMPROVE, EMEP, EANET) in the polluted Northern Hemisphere. The differences between ISORROPIA II v2.3 and ISORROPIA-lite were minimal in all comparisons with the normalized mean absolute difference for the concentrations of all major aerosol components being less than 10 % even when different phase state assumptions were used. The most notable differences were lower aerosol concentrations predicted by
30 ISORROPIA-lite in regions with relative humidity in the range of 20% to 60% compared to the predictions of ISORROPIA II v2.3 in stable mode. The comparison against observations yielded satisfactory agreement especially over the US and Europe, but higher deviations over East Asia, where the overprediction of EMAC for nitrate was as high as 4 µg m^{-3} (~ 20%). The mean annual aerosol pH predicted by ISORROPIA-lite was on average less than a unit lower than ISORROPIA II v2.3 in stable mode, mainly for coarse mode
35 aerosols over Middle East. The use of ISORROPIA-lite accelerated EMAC by 5 % compared to the use of ISORROPIA II v2.3 even if the aerosol thermodynamic calculations consume a relatively small fraction of the EMAC computational time. ISORROPIA-lite can therefore be a reliable and computationally effective replacement of the previous thermodynamic module in EMAC.

40 **Keywords:** atmospheric aerosols, aerosol thermodynamics, nitrate, acidity, aerosol phase state.

1. Introduction

Aerosols in the atmosphere have a significant impact on climate and air pollution. They contribute to the deterioration of air quality, especially in heavily industrialised regions, leading to increased
45   mortality rates and decreased life expectancy (Heroux et al., 2015). Particulate matter with diameter less than 2.5 μm ($PM_{2.5}$) is the largest contributor to stroke, cancer, heart conditions and chronic obstructive pulmonary diseases (Brook et al., 2010; Pope et al., 2011) with ambient pollution causing approximately 4.2 million premature deaths in 2019 alone (WHO, 2022). Tarin-Carrasco et al. (2021) predicted that mortality rates in Europe due to air pollution could increase
50   in the next thirty years in the more extreme emission scenarios (e.g., RCP8.5). Aerosols affect climate by acting as cloud condensation nuclei and by altering cloud lifetime and optical properties (Andreae et al., 2005; Klingmüller et al., 2020). They also affect the energy balance of our planet by reflecting additional solar radiation back to space and thus cooling the atmosphere or by absorbing solar radiation warming the atmosphere (Klingmüller et al., 2019; Miinalainen et al.,
55   2021). Some major inorganic aerosol components also affect various ecosystems. For example, nitrates and sulfates can harm flora by lessening its lifetime and variety (Honour et al., 2009; Manisalidis et al., 2020), and can affect wildlife by causing water eutrophication (Doney et al., 2007). A critical property of atmospheric particles that regulates their impacts on clouds and ecosystems is their acidity (Karydis et al., 2021). Depending on its levels, acidity can affect air
60   quality and human health (Lelieveld et al., 2015) but also the aerosols' hygroscopic characteristics (Karydis et al., 2016). The aerosol pH also drives the partitioning of semi-volatile inorganic components between the gas and aerosol phases (Nenes et al., 2020). Finally, aerosol acidity plays a role in the activation of halogens in aerosols (Saiz-Lopez and von Glasow, 2012), their toxicity (Fang et al., 2017) and also in secondary organic aerosol formation (Marais et al., 2016).
65   Sulfate is the most important component of $PM_{2.5}$ inorganic aerosol, since it contributes the most in terms of global mass burden (Szopa et al., 2021) and aerosol optical depth (AOD) (Myhre et al., 2013). Nitrate contribution to the $PM_{2.5}$ aerosol composition is also important in several areas (e.g. Europe, North America, East Asia) and seasons (He et al., 2001; Silva et al., 2007; Weagle et al., 2018; Tang et al., 2021). The quantification of nitrate partitioning between
70   the gas and particulate phases is challenging partly because it is affected by meteorology (temperature, relative humidity) and all ionic aerosol components, but also due to the lack of observations to constrain the composition of the gas-phase components and the size-distribution of the particulate phase. Nitrate in the form of ammonium nitrate is mainly found in the fine mode (e.g. $PM_{2.5}$) (Putaud et al., 2010). This is especially the case over polluted regions where there is
75   enough ammonia remaining after the neutralization of sulfate (Karydis et al., 2011; Karydis et al., 2016). In coastal and desert areas, nitrate is formed mainly by reactions of HNO_3 with sea salt and dust particles (Savoie and Prospero, 1982; Wolff, 1984; Karydis et al., 2016) and therefore is found mainly in the coarse particles. The importance of nitrate in the troposphere is expected to increase in the following decades because SO_2 emissions are anticipated to drop while NH_3 emissions to
80   increase (Fu et al., 2017; Chen et al., 2019; Xu et al., 2020). With decreased SO_2 concentrations, less ammonia is required to neutralize the sulfates and therefore more is available for ammonium nitrate formation (Tsimpidi et al., 2007).

There have been several thermodynamical models developed in the last decades to calculate the inorganic aerosol concentrations and composition in the atmosphere. Two of the first were EQUIL and KEQUIL developed by Bassett and Seinfeld (1983). Then the MARS model was developed by Saxena et al. (1986) with the aim of reducing the computational time required in order to be incorporated into larger scale chemical transport models. MARS was the first model to divide the composition domain into smaller sub-domains aiming to reduce the number of equations needed to be solved. Then the SEQUILIB model by Pilinis and Seinfeld (1987) was the first to incorporate sodium and chloride and the corresponding salts in the simulated aerosol system. Further developments included EQUISOLV by Jacobson et al. (1996) as well as SCAPE by Kim et al. (1993), which simulated temperature dependent deliquescence following Wexler and Seinfeld (1991) and predicted the presence of liquid phase aerosols even at low relative humidity (RH). E-AIM is another benchmark thermodynamic model which instead of solving algebraic equations for equilibrium, uses the minimization of the Gibbs Free Energy approach (Wexler and Clegg, 2002). Later versions of E-AIM also include selected organic aerosol components (Clegg et al., 2003). Furthermore, AIOMFAC is a model that utilizes organic-inorganic interactions in aqueous solutions in order to calculate activity coefficients up to high ionic strengths (Zuend et al., 2008) and is based on the LIFAC model by Yan et al. (1999). Further developments in AIOMFAC include a wider variety of organic compounds (Zuend et al., 2011).

Nenes et al. (1998) developed the ISORROPIA model in an effort to increase computational efficiency while maintaining the accuracy of the calculations. The system simulated by ISORROPIA included NH_4^+, Na^+, Cl^-, NO_3^-, SO_4^{2-} and H_2O. ISORROPIA also contains the temperature dependent equations for deliquescence by Wexler and Seinfeld (1991) and is computationally efficient so that it can be incorporated in 3D atmospheric models. In ISORROPIA, the aerosol state is predicted as a weighted mean value of the dry and wet states. The weighting factors depend on ambient RH, the mutual deliquescence relative humidity (MDRH) and the deliquescence relative humidity (DRH) of the most hygroscopic salt in the mixture. An improved version of ISORROPIA including the mineral ions K^+, Ca^{2+}, and Mg^+, called ISORROPIA II, was developed by Fountoukis and Nenes (2007). The model gained in computational efficiency by performing different calculations for different atmospheric chemical composition regimes and by using pre-calculated look-up tables for the activity coefficients. Like E-AIM, ISORROPIA II can solve the thermodynamic equilibrium problem under stable or metastable conditions. In the second case aerosols are assumed to exist only as supersaturated aqueous solutions even at low RH, while in the first the aerosols are able to form solid salts. A very slightly updated version, called ISORROPIA II v2.3 was introduced to improve aerosol pH predictions close to neutral conditions (Song et al., 2018). The newest development of ISORROPIA II, called ISORROPIA-lite, was designed to be even more computationally efficient than its predecessor and to also include the effects that organic aerosol components have on particle water and the semi volatile inorganic aerosol species partitioning (Kakavas et al., 2022).

This study aims to evaluate the newly developed ISORROPIA-lite thermodynamic module within the EMAC global climate and chemistry model and to explore any discrepancies on a global scale, by utilizing different aerosol phase states. For this reason, our analysis explores the differences in the results between ISORROPIA-lite and ISORROPIA II over diverse conditions and environments. In Section 2 the model configuration and the treatment of inorganic aerosols

thermodynamics is presented. In Sections 3 and 4 the results and comparisons between the simulations are analyzed and in Section 5 the major conclusions are presented.

2. Model Configuration

2.1 EMAC model setup

130   The EMAC (ECHAM5/MESSy) model is a global atmospheric chemistry and climate model (Jockel et al., 2006). It includes a series of submodels and links them via the Modular Earth Submodel System (Jockel et al., 2005) to the base model (core) that is the 5th generation European Center Hamburg general circulation model (Roeckner et al., 2006). Gas-phase chemistry is simulated by MECCA (Sander et al., 2019) with a simplified scheme similar to the one used in
135   CCMI (Chemistry-Climate Model Initiative) like in Jockel et al. (2016). Aerosol microphysics along with gas/aerosol partitioning are treated by GMXe in which the aerosols are differentiated between soluble and insoluble modes with a total of seven lognormal modes (Pringle et al., 2010). The soluble mode contains the nucleation, Aitken, accumulation, and coarse size ranges while the insoluble mode lacks only the nucleation size range. Transfer of material between the insoluble
140   and soluble modes is calculated in two processes. After coagulation, when a hydrophobic and a hydrophilic particle coagulate the resulting mass is assumed to reside in the hydrophilic mode and also when soluble material condenses onto a hydrophobic particle (after gas/aerosol partitioning) it is again transferred to the hydrophilic mode (Pringle et al., 2010). Wet deposition of gases and aerosols is described by SCAV (Tost et al., 2006; 2007), dry deposition via DRYDEP (Kerkweg
145   et al., 2006) and gravitational sedimentation of aerosols by SEDI (Kerkweg et al., 2006). Cloud properties and microphysics are calculated by the CLOUD submodel (Roeckner et al., 2006) utilizing the detailed two-moment liquid and ice-cloud microphysical scheme of Lohmann and Ferrachat (2010) and considering a physically based treatment of the processes of liquid (Karydis et al., 2017) and ice crystals (Bacer et al., 2018) activation. The organic aerosol composition and
150   evolution in the atmosphere is calculated by the ORACLE submodel (Tsimpidi et al., 2014; 2018).

The model simulations in this work were nudged towards actual meteorology using ERA05 data (Hersbach et al., 2020). For the purposes of this study the spectral resolution applied within EMAC was the T63L31 which corresponds to a grid resolution of 1.875^{o} x 1.875^{o}, covering vertically altitudes up to 25 km with a total of 31 layers. The simulations were all done for the
155   period 2009-2010, with 2009 representing the model spin-up period.

Anthropogenic emissions of aerosols and aerosol precursors were based on the EDGARv4.3.2 inventory (Crippa et al., 2018). Open biomass burning emissions were derived by the GFEDv3.1 database (van der Werf et al., 2010), and natural emissions of NH_3 (volatilization from soils and oceans) were based on the GEIA database (Bouwman et al., 1997). SO_2 emissions
160   by volcanic eruptions are based on the AEROCOM dataset (Dentener et al., 2006), as are emissions of sea spray aerosols using the chemical composition proposed by Seinfeld and Pandis (2016). Biogenic emissions of NO from soils are calculated online according to the algorithm of Yienger and Levy (1995) while NO_x produced by lightning is also calculated online based on the parameterization of Grewe et al. (2001). Oceanic emissions of DMS are calculated online by the

165   AIRSEA submodel (Pozzer et al., 2006). Finally, the dust emission fluxes are calculated online according to Astitha et al. (2012), by taking into account the meteorological information for each grid cell (i.e., temperature and relative humidity) as well as the different thresholds of friction velocities above which suspension of dust particles takes place. The emissions of crustal ions (Ca^{2+}, Mg^+, K^+ and Na^+) are estimated as a fraction of the total dust flux based on the soil chemical
170   composition of each individual grid cell (Karydis et al., 2016; Klingmüller et al., 2018).

2.2 Inorganic aerosol thermodynamics treatment

In this study, the ISORROPIA-lite aerosol thermodynamic model has been implemented into the EMAC as part of the GMXe submodel in order to efficiently calculate the equilibrium partitioning of the inorganic species between gas and aerosol phases. Furthermore, ISORROPIA II v2.3 is used
175   to replace ISORROPIA II v1 in the model.

Kinetic limitations in the partitioning need to be taken into consideration because only fine aerosols are able to achieve equilibrium within the time frame of one model time step, which in this study equals to 10 minutes. Therefore, the partitioning calculation is done in two stages according to Pringle et al. (2010). First the amount of the gas-phase species that is able to
180   kinetically condense onto the aerosol phase within the model time step is calculated by assuming diffusion limited condensation (Vignati et al., 2004). Then in the second stage, the partitioning between this gas phase material and the aerosol phase is performed.

According to Kakavas et al. (2022), ISORROPIA-lite features two main modifications in its code, with regard to ISORROPIA II v2.3 (Song et al., 2018) and ISORROPIA II v1 (Fountoukis
185   and Nenes, 2007). First, the routines related to the stable case have been removed, since only the metastable case is considered. Furthermore, for the calculation of the binary activity coefficients, ISOROPIA-lite uses the tabulated binary activity coefficient data for each salt by Kusik-Meissner instead of computing them online, by combining the Kusik and HP (1978) model for specific ionic pairs with the Bromley (1973) activity coefficients mixing rule for multicomponent mixtures. This
190   second modification is the major contributor to the computational speed-up provided by ISORROPIA-lite, which in an offline estimation was reported to be around 35% (Kakavas et al., 2022). Another important modification is that the effect of organic aerosol water on the inorganic semi volatile aerosol components is included. This consideration slightly increases the aerosol pH but more significantly drives the phase partitioning towards the aerosol phase in order to satisfy
195   equilibrium conditions (Kakavas et al., 2022). However, this feature of ISORROPIA-lite was not used in the present study, as the water uptake by organics is treated by other parts of the GMXe aerosol microphysics submodel in the EMAC global model. The effects of the secondary organic aerosol on aerosol water and nitrate partitioning are discussed by Kakavas et al. (2023).

In the updated version of the GMXe submodel, the users have the option to select between
200   ISORROPIA-lite and ISORROPIA II v2.3 to perform EMAC simulations depending on the application and the desired phase state assumption. While ISORROPIA-lite utilizes the metastable approach exclusively, ISORROPIA II v2.3 utilizes both and has the stable approach as default.

3. Evaluation of New Aerosol Thermodynamic Modules within EMAC

For reasons of clarity, from this point forward both in the main text as well as in any figure
205   captions, whenever different aerosol sizes are mentioned, total suspended particles (TSP) refer to
the sum of the 4 lognormal size modes of the aerosol microphysics submodel (i.e. nucleation,
Aitken, accumulation and coarse mode), fine aerosols refer to the sum of the 3 smaller size modes
(nucleation, Aitken and accumulation mode) and coarse aerosols refer to the largest size mode of
the model exclusively.

210   **3.1 Comparison of ISORROPIA II v1 against ISORROPIA II v2.3 in stable
mode**

The first comparison aims to examine how ISORROPIA II v2.3 fares against ISORROPIA II v1
when considering solely the stable assumption, after the latter's replacement in the newer version
of the EMAC model.

215   The differences in global daily mean surface concentrations of NH_4^+, SO_4^{2-}, mineral ions (sum
of Ca^{2+}, K^+, Mg^{+2}), aerosol water in TSP, as well as fine and coarse aerosol NO_3^- as predicted by
the two versions can be seen in Figure 1. The 25th and 75th percentiles of concentration differences
between the two versions for the aerosol water are below 0.2 μg m^{-3} and for the remaining species
they are an order of magnitude less, which translates to differences mostly below 2.5 % for all
220   species. Therefore, the predictions of inorganic aerosol composition of the two versions agree
exceptionally well.

In order to investigate potential differences arising in specific areas, regions affected by high
nitrate concentrations were selected, i.e., Europe, the Tibetan Plateau, Eastern Asia, North America
and the Middle East. The differences in daily mean coarse and fine NO_3^- over these regions are
225   shown in Figure S1. The comparison showed that the differences regarding the 25th and 75th
percentiles are less than 0.05 μg m^{-3} (or less than 2.5 %) between the results of the two
ISORROPIA II versions for both size modes. A statistical analysis of the results reveals that all
differences between the aforementioned species are on average below 2% (Table 1). Therefore,
the replacement of ISORROPIA II v1 by v2.3 in the EMAC model yields only trivial differences
230   in the predicted aerosol ionic composition and water. The following sections focus on the
comparison between the results of ISORROPIA-lite against ISORROPIA II v2.3 (called
ISORROPIA II hereafter for simplicity), both in stable and metastable states.

235

240
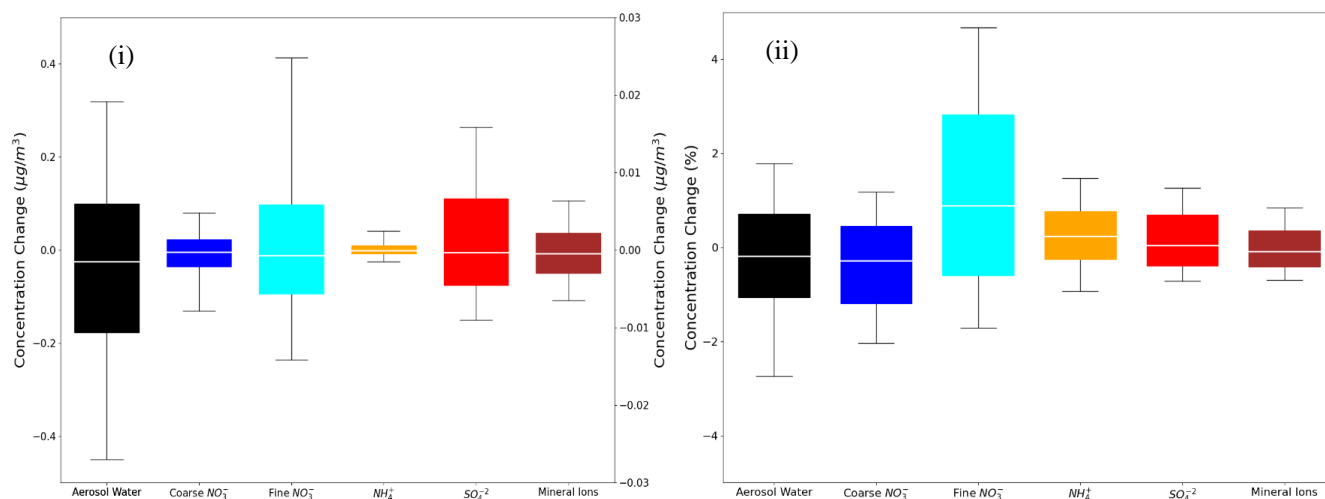
Figure 1: Bar chart plots depicting the 25th, 50th and 75th percentiles (box) of the i) difference and ii) fractional difference in global daily mean surface concentrations of aerosol water (left y-axis), mineral ions, NH_4^+ and SO_4^{2-} in TSP as well as coarse and fine aerosol NO_3^- (right y-axis), as predicted by EMAC using ISORROPIA II v1 and ISORROPIA II v2.3. The 10th and 90th percentiles (whiskers) for each aerosol component are also shown. Both models assume that the aerosol is at its stable state at low RH and a positive change corresponds to higher concentrations by ISORROPIA II v1.

Table 1: Statistical analysis of EMAC-simulated mean annual surface concentrations by employing ISORROPIA II v1 versus ISORROPIA II v2.3, both in **stable mode**. Deviations are given as ISORROPIA II v1 – ISORROPIA II v2.3.

	Mean Difference ($\mu g/m^3$)	Normalized Mean Absolute Difference (%)
Coarse NO_3^-	-0.004	1.2
Fine NO_3^-	-0.005	2.1
HNO_3 (g)	-9×10^{-4}	1.2
NH_4^+	-3×10^{-4}	1.6
SO_4^{2-}	-0.003	0.7
Na^+	0.002	0.5
Ca^{2+}	3×10^{-4}	0.5
K^+	2×10^{-4}	0.5
Mg^+	3×10^{-4}	0.5
Cl^-	0.028	1.6
H_2O	0.040	0.8
H^+	-4×10^{-5}	1.3

3.2 Comparison of ISORROPIA-lite against ISORROPIA II in metastable mode

270

The model results using ISORROPIA-lite are compared first against those using ISORROPIA II in metastable mode in order to determine whether the lite version can produce similar results with the more detailed module in EMAC, under same conditions. Figure 2 depicts the differences of the global daily mean surface concentrations of the same species that were examined before. The

275 comparison yields differences for the 25th and 75th percentiles smaller than 0.5 μg m^{-3} for the aerosol water and smaller than 0.01 μg m^{-3} for the remaining inorganic aerosol components, which translates to differences less than 2% for all species most of the time.

Figure S2 shows the comparison between predicted global daily mean coarse and fine aerosol nitrate concentrations, focusing on the regions with the higher simulated mean annual

280 concentrations. Across all regions, the concentration differences for both size modes are typically lower than 0.1 μg m^{-3} (or less than 3 %) and are mostly found over the Himalayan and East Asian regions.

In Table 2, the statistics of the results for the global surface concentrations for all examined aerosol components, reveal differences that are on average less than 5%. Therefore, ISORROPIA-

285 lite does provide quite similar predictions with ISORROPIA II in the EMAC model, for simulations using the metastable state assumption.
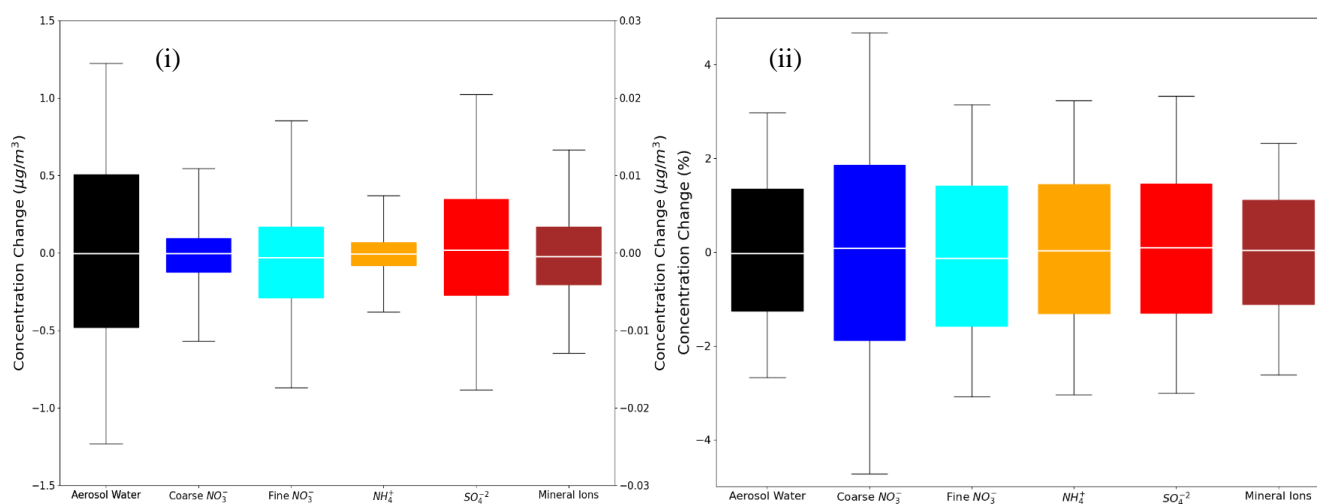
Figure 2 : Bar chart plots depicting the 25th, 50th and 75th percentiles (box) of the i) difference and ii)

300 fractional difference in global daily mean surface concentrations of aerosol water (left y-axis), mineral ions, NH_4^+ and SO_4^{2-} in TSP as well as coarse and fine aerosol NO_3^- (right y-axis) , as predicted by EMAC using ISORROPIA-lite and ISORROPIA II. The 10th and 90th percentiles (whiskers) for each aerosol component are also shown. Both models assume that the aerosol is at its metastable state at low RH and a positive change corresponds to higher concentrations by ISORROPIA-lite.

305 **Table 2:** Statistical analysis of EMAC-simulated mean annual surface concentrations by employing ISORROPIA-lite versus ISORROPIA II, both in **metastable mode**. Bias is given as ISORROPIA lite – ISORROPIA II.

	Mean Difference ($\mu g/m^3$)	Normalized Mean Absolute Difference (%)
Coarse NO_3^-	-7×10^{-4}	1.9
Fine NO_3^-	-2×10^{-4}	2.1
HNO_3	-8×10^{-4}	2.8
NH_4^+	-3×10^{-5}	2.7
SO_4^{2-}	9×10^{-4}	2.3
Na^+	0.004	4.2
Ca^{2+}	4×10^{-4}	2.3
K^+	3×10^{-4}	2.8
Mg^+	7×10^{-4}	3.7
Cl^-	0.008	4.3
H_2O	0.028	1.5
H^+	-1×10^{-5}	4.1

3.3 Evaluation of inorganic aerosol predictions

310 The EMAC predictions using ISORROPIA-lite for $PM_{2.5}$ ammonium, sulfate and nitrate were compared against measurements from three observational networks. The networks cover some of the most polluted areas in the Northern Hemisphere. The EPA CASTNET network (U.S. Environmental Protection Agency Clean Air Status and Trends Network) and the IMPROVE network (Interagency Monitoring of Protected Visual Environments) with 152 stations for nitrate and sulfate and 143 stations for ammonium cover the USA, with IMPROVE concerning mostly
315 rural and/or remote areas. The EMEP network (EMEP Programme Air Pollutant Monitoring Data) includes 9 stations for nitrate and sulfate and 7 for ammonium covering the European region. Finally, the EANET network (The Acid Deposition Monitoring Network in East Asia) with 33 stations measuring all three major aerosol components covers parts of East Asia. The number of
320 stations refers to the year 2010 which is simulated in this work.

Figure 3 depicts the differences between the model-predicted and the observed mean annual concentration values for SO_4^{2-}, NH_4^+ and NO_3^- aerosols, while Tables 3, 4 and 5 contain the overall statistics for the same comparisons. Here, the mean bias (MB), mean absolute gross error (MAGE), normalized mean bias (NMB), normalized mean error (NME), and the root-mean-square
325 error (RMSE) are calculated to assess the model performance. Starting with SO_4^{2-}, the model tends

to underpredict the observations but with mean bias (MB) less than -0.5 µg m^{-3} for Europe and less than -1 µg m^{-3} for USA, capturing both the higher values of the Eastern US and the lower values of the Western US. Its normalized mean error (NME) ranges from 40 to 60 % (Table 3). NH_4^+ is much better simulated by the model over the three regions, where the agreement with observations is high with MB values less than 0.4 µg m^{-3} but with slightly higher NME values (Table 4). Over Eastern Asia, the only important disparity is a slight underprediction of about 2 µg m^{-3} around Hong Kong following the underprediction of SO_4^{2-} over the same area (Fig. 3). Finally, the model tends to overpredict NO_3^- concentrations over the three regions with MB values less than 1 µg m^{-3} albeit with high NME values (Table 5). Over East Asia, with the exception of Hong Kong, the model overestimates the NO_3^- concentrations by about 3 µg m^{-3}, especially in the Wuhan and Guangzhou areas and also around Beijing (Fig. 3). In general, besides Hong Kong, the model overpredicts the concentrations of all three aerosol components examined here in the East Asian region. Potential explanations include the coarse grid resolution used in this work as well as issues related to emissions (Zakoura and Pandis, 2018).
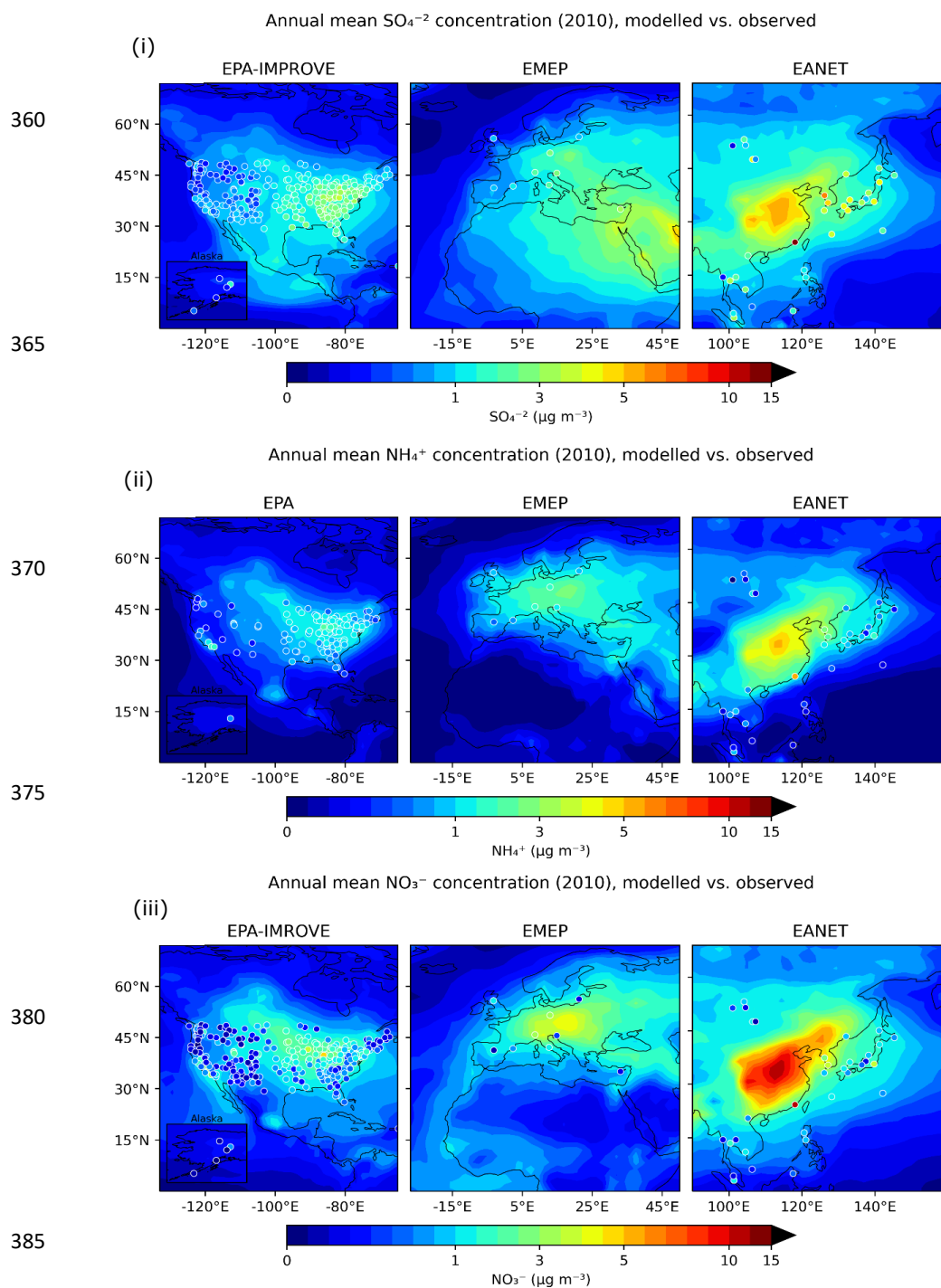
Figure 3: Annual mean surface concentrations of $PM_{2.5}$ i) SO_4^{2-}, ii) NH_4^+, and iii) NO_3^- as simulated by EMAC using ISORROPIA-lite (shaded contours) versus observations of the same species from the IMPROVE, EMEP and EANET networks (colored circles).

Table 3: Statistical evaluation of EMAC predicted surface concentrations of PM$_{2.5}$ SO$_4^{2-}$ using ISORROPIA-lite against observations during 2010.

Network	Number of datasets	Mean Observed (µg m⁻³)	Mean Predicted (µg m⁻³)	MAGE (µg m⁻³)	MB (µg m⁻³)	NME (%)	NMB (%)	RMSE (µg m⁻³)
EPA	1791	2.18	1.28	0.92	-0.90	42	-38	0.93
IMPROVE	1526	1.02	0.92	0.47	-0.10	46	-11	0.73
EMEP	108	1.71	1.27	0.75	-0.44	44	-26	0.91
EANET	353	3.19	1.54	1.95	-1.65	61	-51	2.46

395   **Table 4:** Statistical evaluation of EMAC predicted surface concentrations of PM$_{2.5}$ NH$_4^+$ using ISORROPIA-lite against observations during 2010.

Network	Number of datasets	Mean Observed (µg m⁻³)	Mean Predicted (µg m⁻³)	MAGE (µg m⁻³)	MB (µg m⁻³)	NME (%)	NMB (%)	RMSE (µg m⁻³)
EPA	1660	1.01	1.01	0.50	0.00	49	0	0.72
IMPROVE	-	-	-	-	-	-	-	-
EMEP	84	1.08	1.44	0.63	0.36	59	34	0.75
EANET	360	0.93	1.25	0.69	0.32	74	34	1.25

Table 5: Statistical evaluation of EMAC predicted surface concentrations of PM$_{2.5}$ NO$_3^-$ using ISORROPIA-lite against observations during 2010.

Network	Number of datasets	Mean Observed (µg m⁻³)	Mean Predicted (µg m⁻³)	MAGE (µg m⁻³)	MB (µg m⁻³)	NME (%)	NMB (%)	RMSE (µg m⁻³)
EPA	1762	1.39	1.87	1.06	0.48	76	42	1.65
IMPROVE	1526	0.42	1.18	0.82	0.76	194	175	1.15
EMEP	108	1.15	1.91	1.25	0.76	109	66	1.66
EANET	372	1.32	2.27	1.33	0.95	101	72	2.17

400

3.4 Computational speed-up metrics

405 The computational efficiency and speed-up that ISORROPIA-lite provides compared to ISORROPIA II in both stable and metastable modes were quantified. Table 6 contains the total number of time steps that the EMAC model performed for the same simulation period (i.e., 24 h of CPU-time using 16 nodes) as well as the real time that was needed per individual time step, for each ISORROPIA version. From the difference in the real time required by the model to execute

410 each individual time step, the speed-up of ISORROPIA-lite was found to be close to 4% compared to ISORROPIA II in metastable mode and more than 5 % compared to ISORROPIA II in stable mode. These values are, as expected, lower than the improvement in the computational efficiency that the lite version provides compared to the original version, as found in the offline evaluation, because EMAC contains several other modules that are quite computationally expensive. For

415 example, the gas-phase chemistry (MECCA submodel) as well as wet deposition and liquid phase chemistry (SCAV submodel) are responsible for two thirds of the total computational cost of the global model. As a comparison, the offline speed-up that ISORROPIA-lite provided was calculated to be 35% and when utilized in the regional model PMCAMx 3D it was found to be 10% (Kakavas et al., 2022).

420 **Table 6:** Total number of time steps that EMAC executed in 24 hours of running time and number of seconds needed for each time step, utilizing ISORROPIA-lite and ISORROPIA II (both in Stable & Metastable). The computational speed-up refers to how much quicker (in %) the process is executed by ISORROPIA-lite in comparison to the previous version in both modes.

Simulation	# Time Steps	# Seconds per Timestep	Computational Speed-Up (%)
ISORROPIA-lite	78,071	1.10	-
ISORROPIA II v2.3 (Metastable)	75,403	1.14	3.7
ISORROPIA II v2.3 (Stable)	74,429	1.16	5.5

425

4. Comparison of ISORROPIA-lite Against ISORROPIA II in Stable Mode

In this section, we present a comparison of the ISORROPIA-lite results in metastable mode against those of the ISORROPIA II results in stable mode. Both versions are now available in the latest

430 version of the EMAC model, and the user has the option to utilize either one. This comparison is done in an attempt to quantify the effects of using the metastable case in global atmospheric simulations, and to identify the regions and conditions under which the two assumptions have any significant, but otherwise expected differences. We also investigate differences in the calculated aerosol acidity by the two modules.

4.1 Spatial variability of mean annual aerosol concentrations

For sulfate in TSP the predicted maximum annual average concentration was 7 μg m^{-3} found over East Asia highlighting the large anthropogenic impact over that region, while it was also high (> 5 μg/m^3) in India, Europe, and the Middle East in both simulations (Fig. 4i). Absolute differences for sulfate in TSP were lower than 0.15 μg m^{-3} (< 3%) and found mainly over the polluted northern hemisphere (mainly East USA & Europe) with slightly higher values simulated by ISORROPIA II (Fig. 4ii). The simulated concentrations of NH_4^+ in TSP had maximum annual average values of 6 μg m^{-3} and were found mainly over East Asia, especially around the greater Beijing and Wuhan areas, while India and Europe also exhibited high mean annual values for TSP NH_4^+ (> 3 μg m^{-3}) (Fig. 4iii). The absolute differences for NH_4^+ in TSP between the two model versions are higher over the Himalayan and East Asian regions (in favor of ISORROPIA II) but apparently weaker over USA, the Middle East and Africa (ISORROPIA-lite predicts higher values), although never higher than 0.5 μg m^{-3} (< 5%) (Fig. 4iv). Regarding aerosol NO_3^- concentrations in the coarse mode the maximum annual average of 6 μg m^{-3} was predicted at the Arabian Peninsula (Fig. 4v), while in the fine mode the maximum annual average value of 11 μg m^{-3} was predicted over the metropolitan areas of Wuhan and Guangzhou (Fig. 4vii). Other high annual average concentrations of fine aerosol NO_3^- are found in the Tibetan Plateau and most prominently in heavy industrial regions such as East US, Eastern Asia and Europe (exceeding 4 μg m^{-3} in most of these areas) with the latter two regions contributing high annual average concentrations in the coarse mode as well. The absolute differences for coarse NO_3^- were similar in magnitude to those of NH_4^+ in TSP with the Middle East yielding higher values by ISORROPIA-lite while the opposite is true for Europe and East USA. The absolute differences for fine NO_3^- are higher than those for coarse NO_3^- reaching up to 1.75 μg m^{-3} mainly over the Tibetan Plateau (~ 30%) with ISORROPIA II predicting the higher values. Higher nitrate concentrations were also predicted by ISORROPIA II mainly close to the West coast of South America and North of Atacama Desert. Around those regions as well as the Tibetan Plateau, the relative humidity is often below 50% and 30% respectively (see Fig. 8) and the metastable assumption results in lower nitrate concentrations, in agreement with the findings of Ansari and Pandis (2000). At the same time, ISORROPIA II predicts a higher aerosol fraction for NO_3^- (up to 10%) for the West coast of South America and the Tibetan Plateau. This is not the case for East Asia (Fig. 5ii) although the low sulfate/nitrate ratio of that region, results to an excess of available NH_3 to react with HNO_3 and form ammonium nitrate that would justify the higher fine mode nitrate concentrations by the stable case of ISORROPIA II (Ansari and Pandis, 2000). A higher NO_3^- aerosol fraction (up to 10%) in the Middle East was exhibited by ISORROPIA-lite (Fig. 5ii). This area is characterized by increased mineral ion concentrations and high sulfate to nitrate ratios (Karydis et al., 2016) which led to higher coarse mode nitrate predictions by the metastable case (Ansari and Pandis, 2000), although the maximum difference was only 0.6 μg m^{-3} (Fig. 4vi, 4viii). The differences in coarse and fine NO_3^- among the two versions did not display any strong seasonality as they were only slightly higher during autumn (for East Asia) and winter (for India-Himalayas) (not shown). Regarding the behavior of the mineral ions of Ca^{2+}, K^+, and Mg^{2+} the majority of high concentrations are found around the largest desert regions of the Sahara, Gobi, Atacama and Namib deserts (Figure S3), with Ca^{2+} being evidently the most dominant across all minerals. Furthermore, the absolute difference maps (Fig.

S3) show minimal differences in mean annual surface concentrations (mostly less than 0.5 μg m^{-3}) between the simulations from the two model versions.

480   In the heavily polluted regions (particularly East USA, Europe and East Asia), the particulate NO_3^- dominates compared to the gas phase HNO_3 (Fig. 5i). The fine-mode fraction of the particulate nitrate burden is bigger than the coarse-mode fraction over Eastern Asia, India, Europe, and Eastern USA, while in the large desert areas of the Middle East and the Sahara most of the particulate NO_3^- exists in the coarse mode (Fig. 5iii). The aerosol water fraction is low (<30%) across the most arid regions of Sahara, Atacama, Namib and Gobi, while Europe has the highest continental average aerosol water content in the Northern Hemisphere polluted regions

485 (Fig. 5v). ISORROPIA-lite predicts higher average aerosol water concentration globally since the particles cannot form solids, and the salts remain in a supersaturated metastable solution (Fig. 5vi).

490

495

500

505

510

515

520

525

530

535
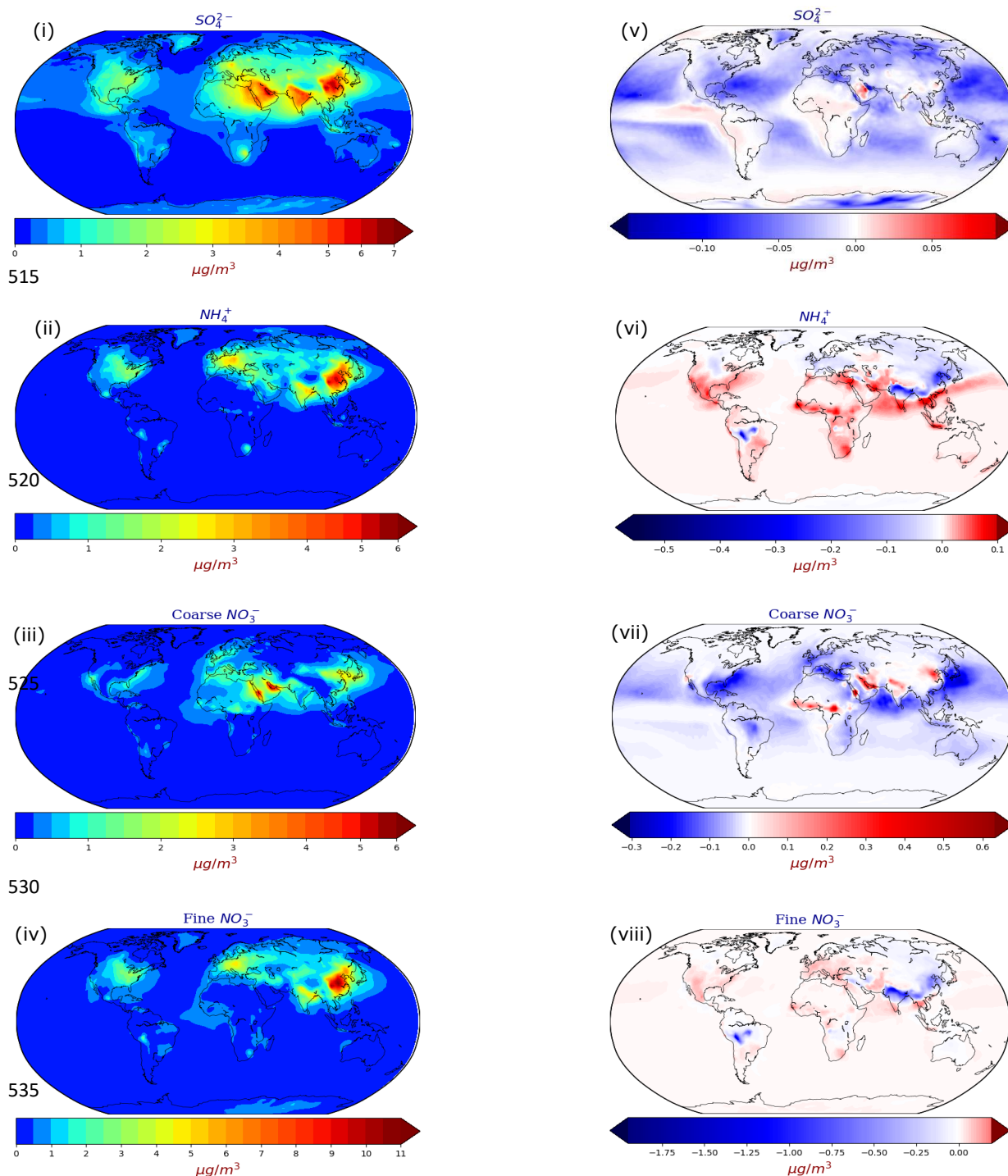
Figure 4 : Annual mean surface concentrations of i) SO_4^{2-} and ii) NH_4^+ in TSP, iii) coarse and iv) fine aerosol NO_3^- as predicted by EMAC using ISORROPIA-lite. Change of the annual mean EMAC-simulated surface concentration of v) NH_4^+ and vi) SO_4^{2-} in TSP, vii) coarse and viii) fine aerosol NO_3^- after employing ISORROPIA II. Positive values in red indicate higher concentrations by ISORROPIA-lite. The models assume different aerosol states.
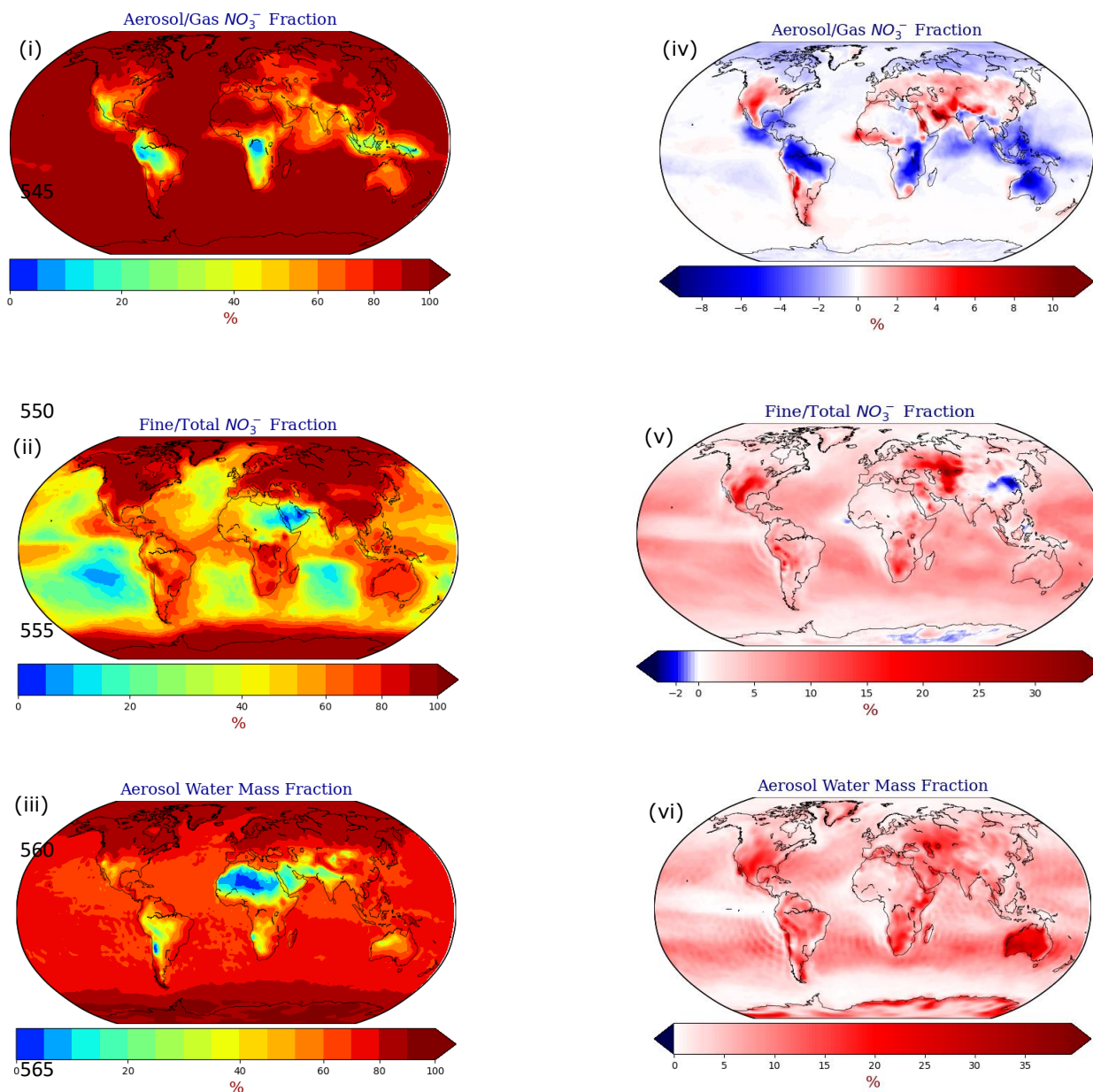
Figure 5 : Annual mean surface fractions of i) aerosol/gas NO₃⁻, ii) fine/total-aerosol NO₃⁻ and iii) aerosol water mass as calculated by EMAC using ISORROPIA-lite. Change of the annual mean EMAC-simulated surface fractions of aerosol/gas iv) NO₃⁻, v) fine/total-aerosol NO₃⁻, and vi) aerosol water mass after employing ISORROPIA II. Positive values in red indicate higher fractions by ISORROPIA-lite. The models assume different aerosol states.

The absolute differences in global daily mean concentrations are less than 0.025 µg m^{-3} (with differences for the 10th and 90th percentiles up to 0.075 µg/m^3) for all species (NH$_4^+$, SO$_4^{2-}$ and Mineral Cations in TSP as well as coarse and fine aerosol NO$_3^-$) except aerosol water in TSP (Figure 6). In that case the absolute differences for the 25th and 75th percentiles are less than 4 µg m^{-3} (with differences for the 10th and 90th percentiles up to 13 µg m^{-3}). This translates to fractional differences for the 25th and 75th percentiles below 20 % (and up to 60 % for differences in the 10th and 90th percentiles) for aerosol water in TSP and coarse NO$_3^-$ aerosol, and below 10 % for differences in the 25th and 75th percentiles (and up to ~ 15 % for differences in the 10th and 90th percentiles) for all the remaining species.

580

585
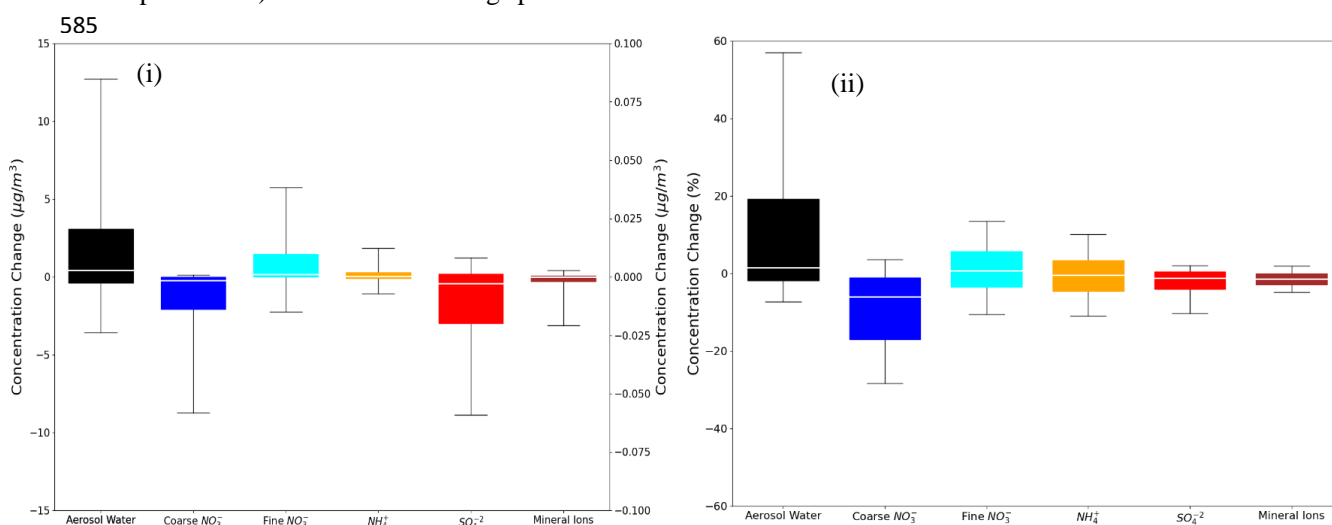
Figure 6 : Bar chart plots depicting the 25th, 50th and 75th percentiles (box) of the i) difference and ii) fractional difference in global daily mean surface concentrations of aerosol water (left y-axis), mineral ions, NH$_4^+$ and SO$_4^{2-}$ in TSP as well as coarse and fine aerosol NO$_3^-$ (right y-axis) , as predicted by EMAC using ISORROPIA-lite and ISORROPIA II. The models assume different aerosol states at low RH and a positive change corresponds to higher concentrations by ISORROPIA-lite.

600

605

610
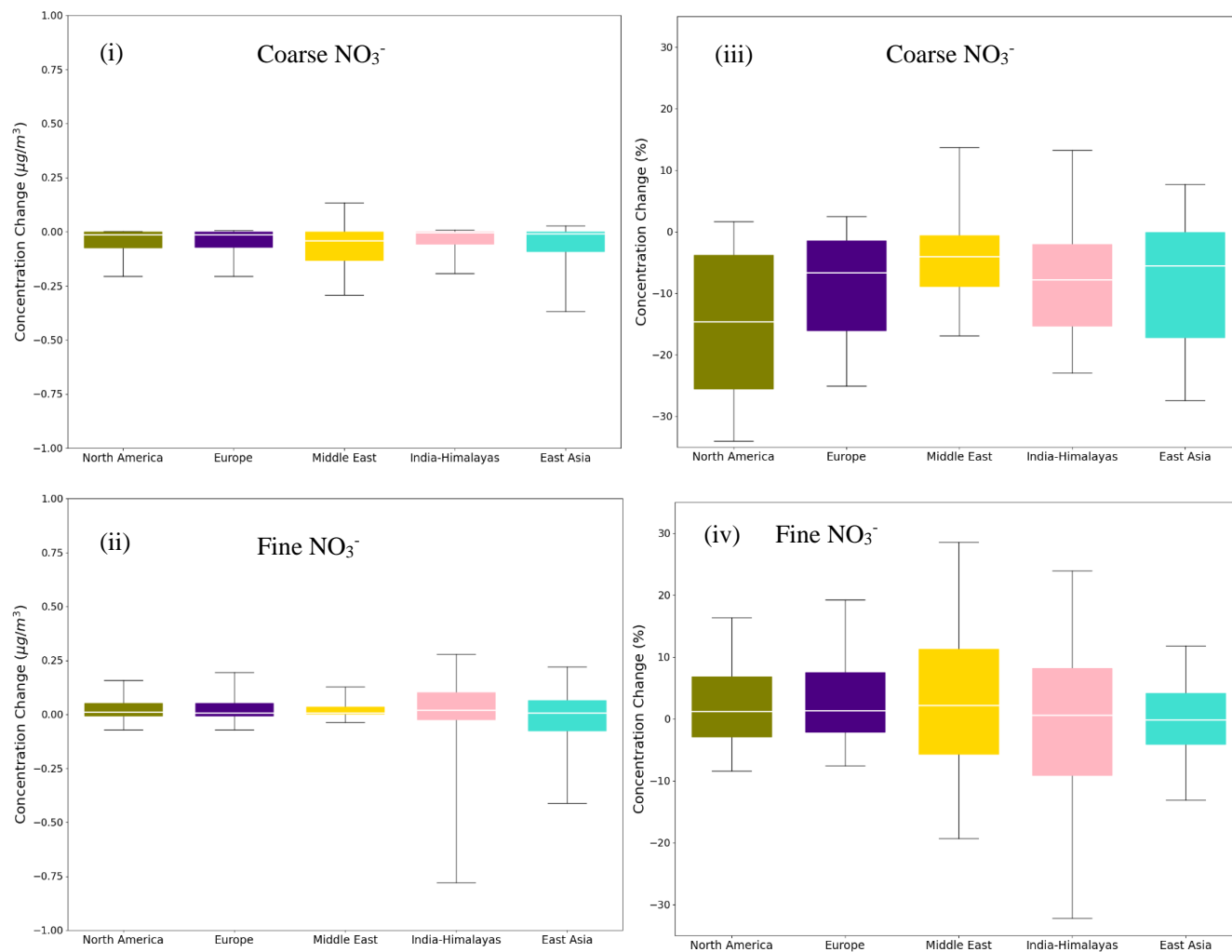
Figure 7: Bar chart plots depicting the 25th, 50th and 75th percentiles (box) of the difference in the global daily mean surface concentrations of i) coarse and ii) fine aerosol NO_3^- for the regions of North America, Europe, Middle East, India-Himalayas and East Asia, as predicted by EMAC using ISORROPIA-lite and ISORROPIA II. The fractional differences in global daily mean surface concentrations of iii) coarse and iv) fine aerosol NO_3^- for the same regions are also shown. The models assume different aerosol states at low RH and a positive change corresponds to higher concentrations by ISORROPIA-lite.

The model results in regions with the highest mean annual load for the fine and coarse aerosol NO_3^- concentrations (see section 3.1) were further analyzed to determine whether the phase state assumption has a large impact on the simulated aerosol nitrate formation (Figure 7). For both coarse and fine daily mean NO_3^- concentrations, Europe and North America are clearly the regions with the smallest differences between the two versions. On the other hand, East Asia and especially the India-Himalayas regions are areas where the differences are the highest with ISORROPIA II predicting higher fine aerosol NO_3^- concentrations while in the Middle East, ISORROPIA-lite is predicting higher coarse mode aerosol NO_3^- concentrations. However, even for these areas the differences are typically below 0.25 µg m^{-3} (25th and 75th percentiles) with the higher differences not exceeding 0.8 µg m^{-3} (10th and 90th percentiles). This translates to fractional differences below

650   25 % (25th and 75th percentiles) for all regions, reaching up to 30 % (10th and 90th percentiles)
mainly in the Tibetan Plateau and the Middle East.

Table 7 contains the statistics for the comparisons of the global daily average surface
concentrations calculated by the two simulations. While all the aerosol component concentrations,
except for aerosol water, are higher for ISORROPIA II, the differences are still quite low.
655   Furthermore, despite the different aerosol phase state assumption by the two versions, the
normalized mean absolute difference remains low for all species (on average < 10 %) except
HNO_3. The overall statistics support the conclusion that on the global scale, the phase state
assumption for low RH does not have a significant impact on the predicted tropospheric aerosol
load. More specifically, ISORROPIA-lite produces a slightly higher tropospheric burden for
660   aerosol NO_3^- than ISORROPIA II (0.875 Tg versus 0.861 Tg, respectively) while the opposite was
the case for HNO_3 (0.921 Tg versus 0.935 Tg). The higher burden of ISORROPIA-lite is due to
the fact that the higher aerosol water content favors the partitioning of HNO_3 to the particulate
phase.

665

670

675

680

Table 7: Statistical analysis of EMAC-simulated mean annual surface concentrations by employing ISORROPIA-lite in **metastable mode** versus ISORROPIA II in **stable mode**. Bias is given as ISORROPIA lite – ISORROPIA II.

	Mean Difference ($\mu g/m^3$)	Normalized Mean Absolute Difference (%)
Coarse NO_3^-	-0.033	6.2
Fine NO_3^-	-0.025	7.6
HNO_3	-0.012	12.6
NH_4^+	-0.004	6.3
SO_4^{2-}	-0.012	3.0
Na^+	-0.066	6.0
Ca^{2+}	-0.011	2.0
K^+	-0.006	2.2
Mg^+	-0.012	3.0
Cl^-	-0.095	6.6
H_2O	1.320	3.6
H^+	-6×10^{-4}	5.5
pH Accumulation	-0.06 (pH)	2.3
pH Coarse	0.03 (pH)	2.3

4.2 Relative humidity dependent behavior of NO_3^- aerosols

The dependence of the differences in nitrate predictions on relative humidity was examined both for fine and coarse particles (Figure 8). The differences between ISORROPIA II and ISORROPIA-lite are higher at intermediate RH ranging from 20% to 60% being more evident in the fine mode aerosol NO_3^- ($> 4 \mu g\ m^{-3}$) and for high annual mean concentrations of coarse mode aerosol NO_3^- ($> 4 \mu g\ m^{-3}$). In this RH range, solid salts can precipitate when the stable equilibrium state is assumed (Seinfeld and Pandis, 2016), while in the metastable state all these salts remain dissolved in water. A region that has often RH in the 20 - 60% range is the Tibetan Plateau which leads to discrepancies of the fine mode particulate nitrate predictions of the two models in this area, while higher coarse mode particulate nitrate concentrations are predicted by ISORROPIA-lite in the Middle East, an area that is also often characterized by intermediate RH. The differences found for coarse mode particulate nitrate in the higher RH ranges of 60 – 100 %, can account for the respective differences that occurred in areas characterized by such RH values (East USA, Europe and East Asia) but concern lower annual mean concentration values ($< 3 \mu g\ m^{-3}$).
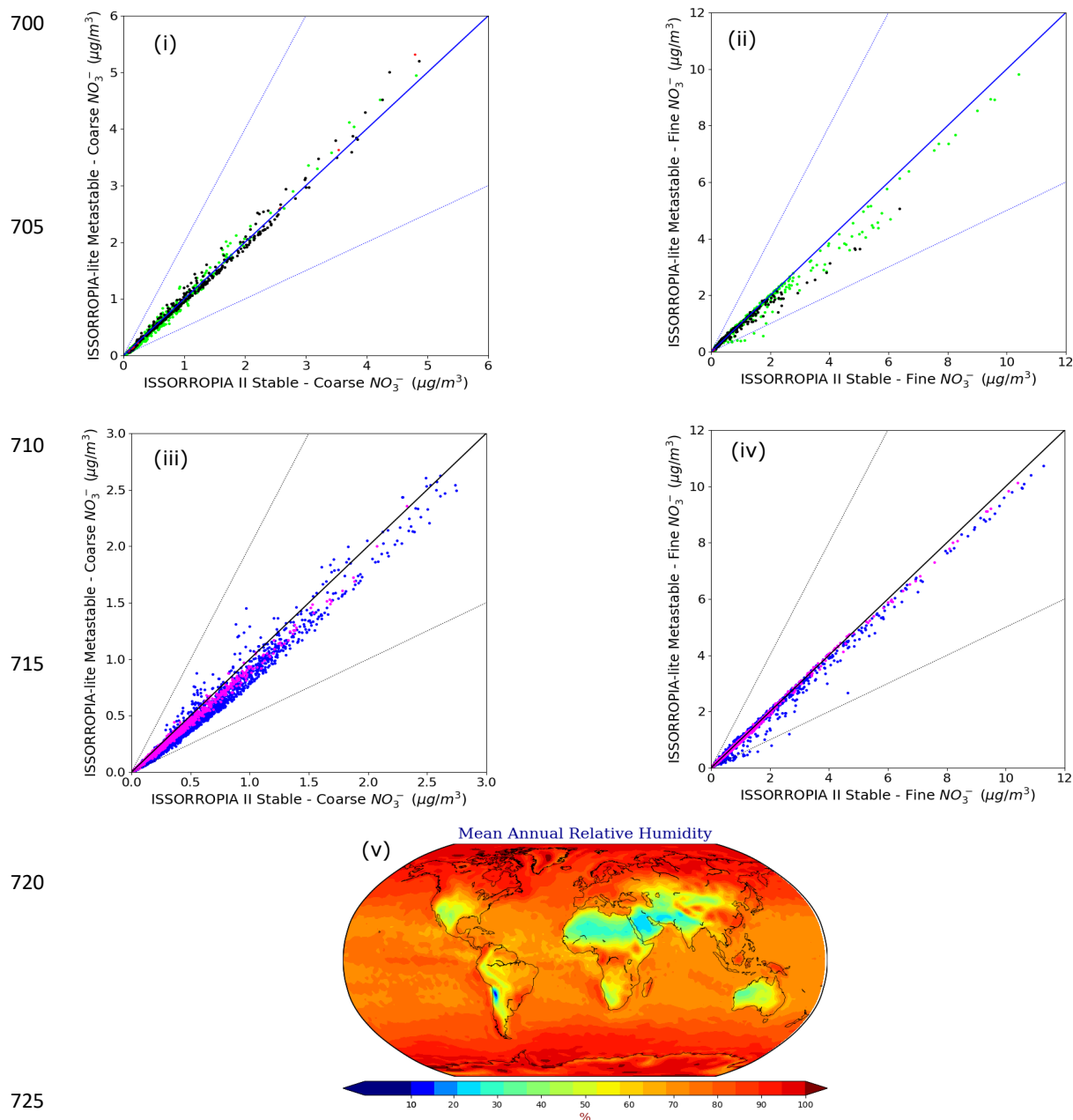
Figure 8: Scatterplots comparing the annual mean surface concentrations of coarse (i, iii) and fine aerosol NO$_3^-$ (ii, iv) for relative humidity ranges of 20-60 % (i, ii) and 60-100 % (iii, iv) as predicted by EMAC using ISORROPIA-lite versus ISORROPIA II. The models assume different aerosol states at low RH. Black points represent the 20-40 % RH range, green points the 40-60 % range, blue points the 60-80 % range and pink points the 80-100 % range. v) Mean annual relative humidity as calculated by EMAC using ISORROPIA-lite.

4.3 Comparison of the estimated aerosol acidity

The estimated aerosol acidity by the two model versions was compared. The pH was computed for the fine and coarse particles, by:

735

$$pH = -log_{10}\left(\frac{[H^+]}{[H2O]}\right) \tag{1}$$

The calculations were performed neglecting the water associated with the organic fraction of aerosols, as they are handled by other parts of the aerosol microphysics submodel GMXe. The average pH was calculated based on the instantaneous H^+ and H_2O values estimated every 5 hours.

740 This is because utilizing daily average values for H^+ and H_2O can result in a low-biased predicted pH of ~2 units globally (Karydis et al., 2021). pH calculations are performed only in cases where there is enough water in the aerosol (instantaneous values exceeding 0.05 μg m^{-3}).

ISORROPIA-lite predicts slightly more acidic particles mainly in the coarse mode (Fig. 9iv). The most significant differences (up to 1 unit) in that size range are located over the Middle

745 East and Arabian Peninsula, while smaller differences can be found in limited parts of the Himalayan and the East Asian regions as well as West USA and the Amazon Basin. These regions are characterized by high mineral cation concentrations and/or low RH. Therefore, the stable state results in increased pH values due to the precipitation of insoluble salts (e.g., $CaSO_4$) out of the aqueous phase. On the other hand, in the metastable state all anions remain in the aqueous phase

750 lowering the particle pH. Differences in accumulation mode particle acidity are not as high (Fig. 9ii). ISORROPIA-lite predicts that accumulation mode particles over heavy industrialized regions such as Southeast Asia, Europe and Eastern USA are moderately acidic with mean pH values in the range of 4 - 5 while exhibiting alkaline behavior in desert areas where the increased levels of mineral ions elevate the pH above 7 (Fig. 9i). Coarse mode particles are in general more alkaline

755 than those in the accumulation mode, with a few exceptions over east US, central Europe, north India and SE Asia (Fig. 9iii). These regions are characterized by high NH_3 concentrations from agricultural activities.

760

765
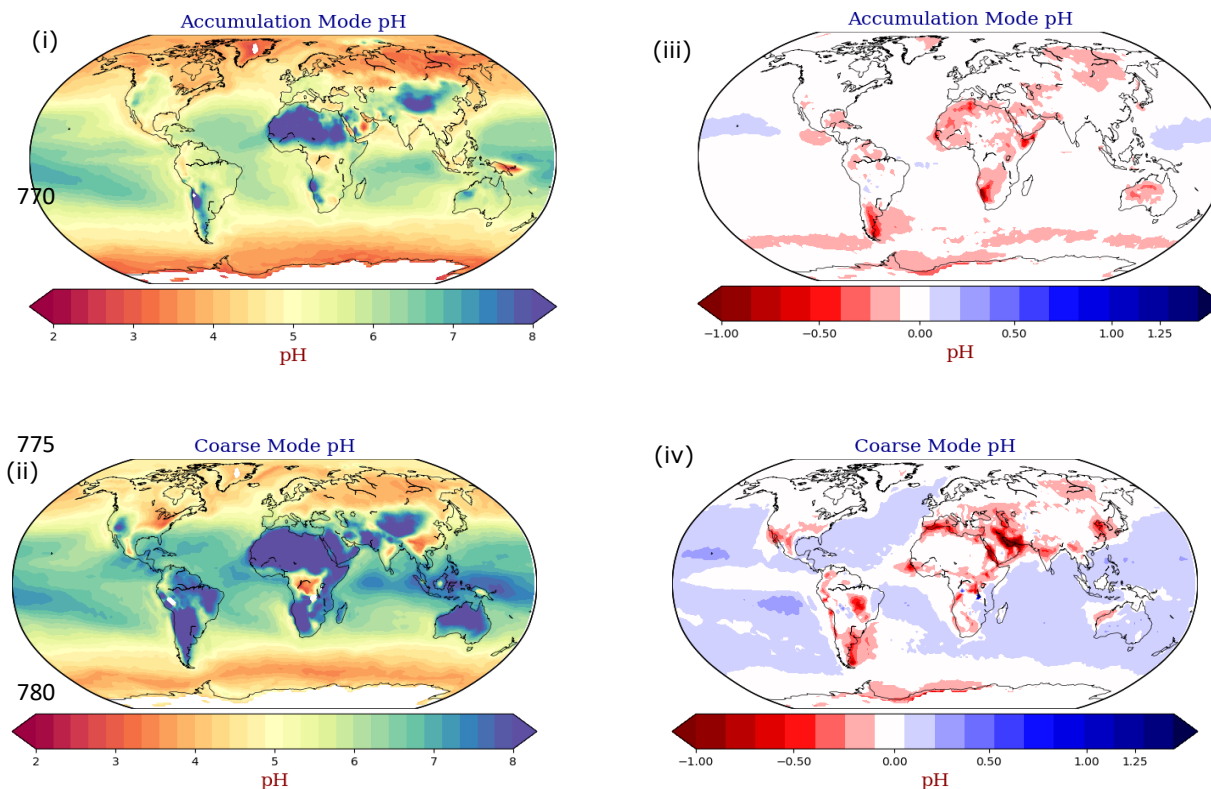
Figure 9: Annual mean EMAC-simulated i) accumulation and ii) coarse mode aerosol pH using
ISORROPIA-lite. Change of the annual mean EMAC-simulated iii) accumulation and iv) coarse mode
aerosol pH after using ISORROPIA II, with negative values in red indicating lower pH by ISORROPIA-
lite. The models assume different aerosol states.

A sensitivity test was performed by switching off all the NH_3 emissions with the aim to
deduce whether there is a buffering mechanism that controls the pH of the accumulation mode
particles more strongly than in the coarse. Figure 10 shows the difference of the mean annual
calculated aerosol pH between the base case (NH_3 emissions present) and the sensitivity case
(without NH_3 emissions). When NH_3 emissions are switched off, the pH of fine PM decreases by
up to 5 units and the particles become a lot more acidic (Fig. 10i). For the coarse mode this effect
is not that strong (pH reduction of up to 2 units) (Fig. 10ii). As expected, this buffering mechanism
is mainly observed across the aforementioned regions where NH_3 concentrations are high, but also
over areas affected by natural NH_3 emissions. This is consistent with the results of Karydis et al.
(2021) who found that in the absence of NH_3, aerosol particles would be extremely acidic in most
of the world.

The differences in the accumulation mode pH calculated by ISORROPIA-lite and
ISORROPIA II are extremely small (i.e., mean difference of 0.06 pH units or 2.3%), and even
smaller for coarse mode pH (Table 7), indicating an overall good agreement between the two
model versions.
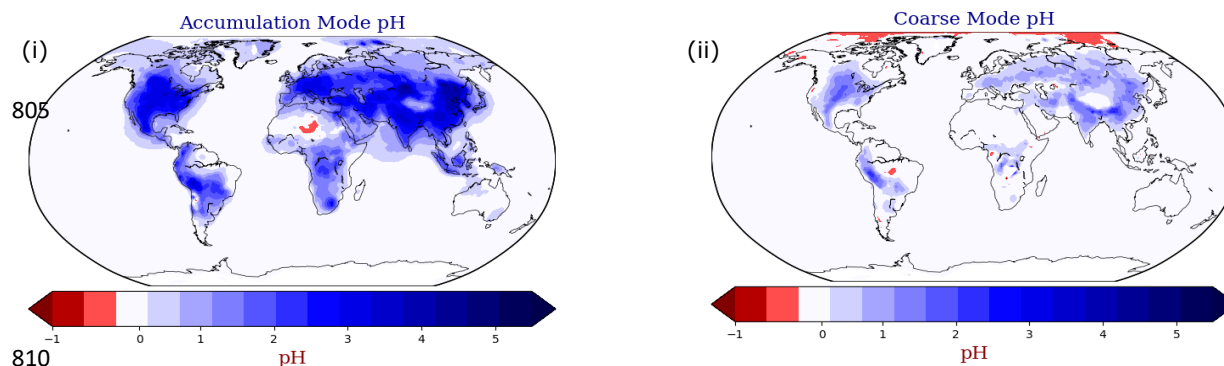
Figure 10: Absolute change of the annual mean EMAC-simulated i) accumulation and ii) coarse mode aerosol pH using ISORROPIA-lite after switching off the NH_3 emissions. Positive values in blue indicate higher aerosol pH when NH_3 is present.

5. Conclusions

This study presents the first results of the implementation of the ISORROPIA-lite thermodynamic module in the EMAC global chemistry and climate model, and is compared to the previous version, ISORROPIA II v2.3, after the latter has successfully replaced ISORROPIA II v1 to improve pH predictions close to neutral conditions.

The results of ISORROPIA II versions 1 and 2.3 both in stable mode, had insignificant differences (<3%) concerning the global predictions of NH_4^+, SO_4^{2-}, mineral ions and aerosol water in TSP concentrations as well as fine and coarse mode aerosol NO_3^-. The comparison of results from ISORROPIA-lite against ISORROPIA II v2.3 in metastable mode, showed also negligible differences (<5%) between all the examined aerosol components on a global scale. The comparison of the ISORROPIA-lite results for $PM_{2.5}$ NH_4^+, SO_4^2, and NO_3^- versus observations from the IMPROVE, EMEP and EANET networks reveals that East Asia is the area with the largest discrepancies. There was satisfactory agreement in Europe and over the US for NH_4^+ and SO_4^{2-}, while ISORROPIA-lite predicted lower concentrations around Hong Kong with a maximum difference of 1.5 μg m^{-3} (~20 %) for these two species. For NO_3^-, the discrepancy was up to 3 μg m^{-3} (~30 %) in the same region, while a difference of about 1.5 μg m^{-3} (~25 %) was found over Central Europe with ISORROPIA-lite predicting the higher values. With the exception of Hong Kong, the model in general overpredicted the concentrations of all three aerosol components over the East Asian region.

A comparison between ISORROPIA-lite in metastable state and ISORROPIA II in stable state was performed to identify potential discrepancies on the EMAC-simulated inorganic aerosol concentrations. These two modules are now both available as different options in the EMAC model. The agreement between the two versions was generally quite good for global daily mean surface concentrations of inorganic aerosols, mineral ions and aerosol water. More specifically mineral ions, SO_4^{2-} and NH_4^+ in TSP had the smallest differences overall, less than 0.5 μg m^{-3} even in localized extreme cases and but in the vast majority less than 0.05 μg m^{-3} (or less than 10%). For coarse NO_3^- aerosols the absolute differences were of similar magnitude with the higher concentrations simulated by ISORROPIA-lite in the Middle East being the most notable. In the

case of fine NO_3^- aerosols, the differences were larger (up to ~ 1.75 μg m^{-3} in local extremes), mainly over the West coast of South America (North of Atacama Desert), the Tibetan Plateau and Eastern Asia regions with higher concentrations simulated by ISORROPIA II but still within ~30%. In Europe and the US, the corresponding differences were less than 0.25 μg m^{-3}. The most important difference was the higher aerosol water calculated by ISORROPIA-lite, especially for relative humidity in the 20% to 60 % range. However, this was less than 5 μg m^{-3} or 20 % in most cases. Therefore, even though local differences are expected in regions where the relative humidity is often in this range, on a global scale choosing a different physical state of the aerosol at lower RH does not have such a big impact.

When the relative humidity ranged from 20 % to 60 %, differences in coarse and fine NO_3^- concentrations predictions among the two versions increased. The highest discrepancies were found in the Tibetan Plateau and the Middle East regions both of which are dominated by such RH values during most of the year. In the first region, the combination of those RH values with mid-range temperatures does not favor nitrate aerosol formation if the aerosol is in the metastable state (ISORROPIA-lite). In the second region, the low RH values result in very low aerosol water predictions for the stable state assumed by ISORROPIA II which hinder the condensation of HNO_3 into the aerosol phase.

ISORROPIA-lite produces slightly more acidic coarse mode aerosols (in comparison to ISORROPIA II) but by less than 1 pH unit on average. The most important differences were found mainly in the Middle East and Arabian Peninsula due to the presence of high mineral cation concentrations. The stable state considered by ISORROPIA II allows the precipitation of insoluble salts and removes anions from the aqueous phase that would otherwise deplete the pH, while this is not the case for the metastable aerosol state considered by ISORROPIA-lite. Furthermore, NH_3 is found to control the aerosol acidity of both fine and coarse mode particles, however, it provides significantly larger buffering capacity to the accumulation mode than to the coarse. This results in slightly more basic accumulation particles than coarse in regions with high NH_3 presence from agricultural activities and low mineral cation concentrations (e.g., Europe).

Finally concerning the computational efficiency that ISORROPIA-lite provides when used by the EMAC global model, a speed-up of close to 4% was achieved compared to ISORROPIA II in metastable state and more than 5% compared to ISORROPIA-II in stable state.

Code and Data Availability

875 The usage of MESSy (Modular Earth Submodel System) and access to the source code is licensed to all affiliates of institutions which are members of the MESSy Consortium. Institutions can become a member of the MESSy Consortium by signing the MESSy Memorandum of Understanding. More information can be found on the MESSy Consortium Website http://www.messy-interface.org. The code developed in this study and all relevant features are
880 available in the commit edb6fcae in the MESSy source code repository which is based on MESSy version 2.56. The ISORROPIA II v2.3 and ISORROPIA-lite v1.0 thermodynamic equilibrium codes are available at https://isorropia.epfl.ch. The data produced in the study are available from the author upon request.

Acknowledgements

885 This work was supported by the project FORCeS funded from the European Union's Horizon 2020 research and innovation program under grant agreement No 821205. The work described in this paper has received funding from the Initiative and Networking Fund of the Helmholtz Association through the project "Advanced Earth System Modelling Capacity (ESM)". The authors gratefully acknowledge the Earth System Modelling Project (ESM) for funding this work by providing
890 computing time on the ESM partition of the supercomputer JUWELS (Alvarez, 2021) at the Jülich Supercomputing Centre (JSC).

Competing Interests

HT acts as a topical editor for GMD but has no further competing interests.

Author Contributions

895 AM and VAK wrote the paper with contributions from all coauthors. VAK planned the research with contributions from AKS, SNP and AN. AN and SNP provided the ISORROPIA-lite model. AM and HT performed the implementation in EMAC. AM performed the simulations and analyzed the results assisted by VAK and APT. APT provided the observations and performed the model evaluation. All the authors discussed the results and contributed to the manuscript.

900

References

905 Alvarez, D.: JUWELS cluster and booster: Exascale pathfinder with modular supercomputing architecture at juelich supercomputing Centre. *Journal of large-scale research facilities JLSRF*, *7*, A183-A183, https://doi.org/10.17815/jlsrf-7-183, 2021.

Andreae, M. O., Jones, C. D., and Cox, P. M.: Strong present-day aerosol cooling implies a hot future. *Nature*, *435*(7046), 1187-1190, https://doi.org/10.1038/nature03671, 2005.

910 Ansari, A. S. and Pandis, S. N.: The effect of metastable equilibrium states on the partitioning of nitrate between the gas and aerosol phases. *Atmospheric Environment*, *34*(1), 157-168, https://doi.org/10.1016/S1352-2310(99)00242-3, 2000.

Astitha, M., Lelieveld, J., Abdel Kader, M., Pozzer, A., and De Meij, A: Parameterization of dust emissions in the global atmospheric chemistry-climate model EMAC: impact of nudging and soil
915 properties. *Atmospheric Chemistry and Physics*, *12*(22), 11057-11083, https://doi.org/10.5194/acp-12-11057-2012, 2012.

Bacer, S., Sullivan, S. C., Karydis, V. A., Barahona, D., Kramer, M. and co-authors: Implementation of a comprehensive ice crystal formation parameterization for cirrus and mixed-phase clouds in the EMAC model (based on MESSy 2.53). *Geoscientific model development, 11*(10), 4021-4041,
920 https://doi.org/10.5194/gmd-11-4021-2018, 2018 .

Bassett, M. and Seinfeld, J. H.: Atmospheric equilibrium model of sulfate and nitrate aerosols. *Atmospheric Environment (1967)*, *17*(11), 2237-2252, https://doi.org/10.1016/0004-6981(83)90221-4, 1983.

Bouwman, A. F., Lee, D. S., Asman, W. A., Dentener, F. J., Van Der Hoek, K. W., and Olivier, J. G. J.: A global
925 high-resolution emission inventory for ammonia. *Global biogeochemical cycles*, *11*(4), 561-587, https://doi.org/10.1029/97GB02266, 1997.

Bromley, L. A.: Thermodynamic properties of strong electrolytes in aqueous solutions. *AIChE journal*, *19*(2), 313-320, https://doi.org/10.1002/aic.690190216, 1973.

Brook, R. D., Rajagopalan, S., Pope, C. A., Brook, J. R., Bhatnagar, A. and co-authors: Particulate matter air
930 pollution and cardiovascular disease: an update to the scientific statement from the American Heart Association. *Circulation*, *121*(21), 2331-2378, https://doi.org/10.1161/CIR.0b013e3181dbece1, 2010.

Chen, Y., Shen, H., and Russell, A. G.: Current and future responses of aerosol pH and composition in the US to declining SO2 emissions and increasing NH3 emissions. *Environmental Science &*
935 *Technology*, *53*(16), 9646-9655, https://doi.org/10.1021/acs.est.9b02005, 2019.

Clegg, S. L., Seinfeld, J. H., and Edney, E. O.: Thermodynamic modelling of aqueous aerosols containing electrolytes and dissolved organic compounds. II. An extended Zdanovskii–Stokes–Robinson approach. *Journal of aerosol science*, *34*(6), 667-690, https://doi.org/10.1016/S0021-8502(03)00019-3, 2003.

940 Crippa, M., Guizzardi, D., Muntean, M., Schaaf, E., Dentener, F. and co-authors: Gridded emissions of air pollutants for the period 1970–2012 within EDGAR v4. 3.2. *Earth Syst. Sci. Data*, *10*(4), 1987-2013, https://doi.org/10.5194/essd-10-1987-2018, 2018.

Dentener, F., Kinne, S., Bond, T., Boucher, O., Cofala, J. and co-authors: Emissions of primary aerosol and precursor gases in the years 2000 and 1750 prescribed data-sets for AeroCom. *Atmospheric*
945 *Chemistry and Physics*, *6*(12), 4321-4344, https://doi.org/10.5194/acp-6-4321-2006, 2006.

Doney, S. C., Mahowald, N., Lima, I., Feely, R. A., Mackenzie, F. T., Lamarque, J. F., and Rasch, P. J.: Impact of anthropogenic atmospheric nitrogen and sulfur deposition on ocean acidification and the inorganic carbon system. *Proceedings of the National Academy of Sciences*, *104*(37), 14580-14585, https://doi.org/10.1073/pnas.0702218104, 2007.

950 EMEP Programme Air Pollutant Monitoring Data, available at : https://projects.nilu.no/ccc/index.html

Fang, T., Guo, H., Zeng, L., Verma, V., Nenes, A., and Weber, R. J.: Highly acidic ambient particles, soluble metals, and oxidative potential: a link between sulfate and aerosol toxicity. *Environmental science & technology*, *51*(5), 2611-2620, https://doi.org/10.1021/acs.est.6b06151, 2017.

Fountoukis, C. and Nenes, A.: ISORROPIA II: a computationally efficient thermodynamic equilibrium model for K+–Ca 2+–Mg 2+–NH 4+–Na+–SO 4 2––NO 3––Cl––H 2 O aerosols. *Atmospheric Chemistry and Physics*, *7*(17), 4639-4659, https://doi.org/10.5194/acp-7-4639-2007, 2007.

Fu, X., Wang, S., Xing, J., Zhang, X., Wang, T., and Hao, J.: Increasing ammonia concentrations reduce the effectiveness of particle pollution control achieved via SO2 and NO X emissions reduction in east China. *Environmental Science & Technology Letters*, *4*(6), 221-227, https://doi.org/10.1021/acs.estlett.7b00143, 2017.

Grewe, V., Brunner, D., Dameris, M., Grenfell, J. L., Hein, R., Shindell, D., and Staehelin, J.: Origin and variability of upper tropospheric nitrogen oxides and ozone at northern mid-latitudes. *Atmospheric Environment*, *35*(20), 3421-3433, https://doi.org/10.1016/S1352-2310(01)00134-0, 2001.

He, K., Yang, F., Ma, Y., Zhang, Q., Yao, X., Chan, C. K., Cadle, S., Chan, T., and Mulawa, P.: The characteristics of PM2. 5 in Beijing, China, *Atmospheric Environment*, 35(29), 4959-4970, https://doi.org/10.1016/S1352-2310(01)00301-6, 2001.

Héroux, M. E., Anderson, H. R., Atkinson, R., Brunekreef, B., Cohen, A., Forastiere, F. and co-authors: Quantifying the health impacts of ambient air pollutants: recommendations of a WHO/Europe project. *International journal of public health*, *60*, 619-627, https://doi.org/10.1007/s00038-015-0690-y, 2015.

Hersbach, H., Bell, B., Berrisford, P., Hirahara, S., Horanyi, A. and co-authors: The ERA5 global reanalysis. *Quarterly Journal of the Royal Meteorological Society*, *146*(730), 1999-2049, https://doi.org/10.1002/qj.3803, 2020.

Honour, S. L., Bell, J. N. B., Ashenden, T. W., Cape, J. N., and Power, S. A.: Responses of herbaceous plants to urban air pollution: effects on growth, phenology and leaf surface characteristics. *Environmental pollution*, *157*(4), 1279-1286, https://doi.org/10.1016/j.envpol.2008.11.049, 2009.

Interagency Monitoring of Protected Visual Environment (IMPROVE), available at : http://vista.cira.colostate.edu/Improve/improve-data/

Jacobson, M. Z., Tabazadeh, A., and Turco, R. P.: Simulating equilibrium within aerosols and nonequilibrium between gases and aerosols. *Journal of Geophysical Research: Atmospheres*, *101*(D4), 9079-9091, https://doi.org/10.1029/96JD00348, 1996.

Jöckel, P., Sander, R., Kerkweg, A., Tost, H., and Lelieveld, J.: the modular earth submodel system (MESSy)- a new approach towards earth system modeling. *Atmospheric Chemistry and Physics*, *5*(2), 433-444, https://doi.org/10.5194/acp-5-433-2005, 2005.

Jockel, P., Tost, H., Pozzer, A., Bruhl, C., Buchholz, J. and co-authors: The atmospheric chemistry general circulation model ECHAM5/MESSy1: consistent simulation of ozone from the surface to the mesosphere. *Atmospheric Chemistry and Physics*, *6*(12), 5067-5104, https://doi.org/10.5194/acp-6-5067-2006, 2006.

Jockel, P., Tost, H., Pozzer, A., Kunze, M., Kirner, O. and co-authors: Earth system chemistry integrated modelling (ESCiMo) with the modular earth submodel system (MESSy) version 2.51. *Geoscientific Model Development*, *9*(3), 1153-1200, https://doi.org/10.5194/gmd-9-1153-2016, 2016.

Kakavas, S., Pandis, S. N., and Nenes, A.: ISORROPIA-Lite: A Comprehensive Atmospheric Aerosol Thermodynamics Module for Earth System Models. *Tellus B: Chemical and Physical Meteorology*, *74*(2022), https://doi.org/10.16993/tellusb.33, 2022.

Kakavas, S., Pandis, S., and Nenes, A.: Effects of Secondary Organic Aerosol Water on fine PM levels and composition over US. *Atmospheric Chemistry and Physics [preprint]*, https://doi.org/10.5194/acp-2022-815, 16 January 2023.

1000   Karydis, V. A., Tsimpidi, A. P., Lei, W., Molina, L. T., and Pandis, S. N.: Formation of semivolatile inorganic aerosols in the Mexico City Metropolitan Area during the MILAGRO campaign. *Atmospheric Chemistry and Physics*, *11*(24), 13305-13323, https://doi.org/10.5194/acp-11-13305-2011, 2011.

Karydis, V. A., Tsimpidi, A. P., Pozzer, A., Astitha, M., and Lelieveld, J.: Effects of mineral dust on global atmospheric nitrate concentrations. *Atmospheric Chemistry and Physics*, *16*(3), 1491-1509,
1005   https://doi.org/10.5194/acp-16-1491-2016, 2016.

Karydis, V. A., Tsimpidi, A. P., Bacer, S., Pozzer, A., Nenes, A., and Lelieveld, J.: Global impact of mineral dust on cloud droplet number concentration. *Atmospheric Chemistry and Physics*, *17*(9), 5601-5621, https://doi.org/10.5194/acp-17-5601-2017, 2017.

Karydis, V. A., Tsimpidi, A. P., Pozzer, A., and Lelieveld, J.: How alkaline compounds control atmospheric
1010   aerosol particle acidity. *Atmospheric Chemistry and Physics*, *21*(19), 14983-15001, https://doi.org/10.5194/acp-21-14983-2021, 2021.

Kerkweg, A., Buchholz, J., Ganzeveld, L., Pozzer, A., Tost, H., and Jöckel, P.: An implementation of the dry removal processes DRY DEPosition and SEDImentation in the Modular Earth Submodel System (MESSy). *Atmospheric Chemistry and Physics*, *6*(12), 4617-4632, https://doi.org/10.5194/acp-6-
1015   4617-2006, 2006.

Kim, Y. P., Seinfeld, J. H., and Saxena, P.: Atmospheric gas-aerosol equilibrium I. Thermodynamic model. *Aerosol Science and Technology*, *19*(2), 157-181, https://doi.org/10.1080/02786829308959628, 1993.

Klingmüller, K., Metzger, S., Abdelkader, M., Karydis, V. A., Stenchikov, G. L., Pozzer, A., and Lelieveld, J.:
1020   Revised mineral dust emissions in the atmospheric chemistry–climate model EMAC (MESSy 2.52 DU_Astitha1 KKDU2017 patch). *Geoscientific Model Development*, *11*(3), 989-1008, https://doi.org/10.5194/gmd-11-989-2018, 2018.

Klingmüller, K., Lelieveld, J., Karydis, V. A., and Stenchikov, G. L.: Direct radiative effect of dust–pollution interactions. *Atmospheric chemistry and physics*, *19*(11), 7397-7408,
1025   https://doi.org/10.5194/acp-19-7397-2019, 2019.

Klingmüller, K., Karydis, V. A., Bacer, S., Stenchikov, G. L., and Lelieveld, J.: Weaker cooling by aerosols due to dust–pollution interactions. *Atmospheric Chemistry and Physics*, *20*(23), 15285-15295, https://doi.org/10.5194/acp-20-15285-2020, 2020 .

Kusik, C. and HP, M. 1978. Electrolyte Activity Coefficients in Inorganic Processing. AIChE Symp. Series,
1030   173, 14-20, 1978.

Lelieveld, J., Evans, J. S., Fnais, M., Giannadaki, D., and Pozzer, A.: The contribution of outdoor air pollution sources to premature mortality on a global scale. *Nature*, *525*(7569), 367-371, https://doi.org/10.1038/nature15371, 2015.

Lohmann, U. and Ferrachat, S.: Impact of parametric uncertainties on the present-day climate and on the
1035   anthropogenic aerosol effect. *Atmospheric Chemistry and Physics*, *10*(23), 11373-11383, https://doi.org/10.5194/acp-10-11373-2010, 2010.

Manisalidis, I., Stavropoulou, E., Stavropoulos, A., and Bezirtzoglou, E.: Environmental and health impacts of air pollution: a review. *Frontiers in public health*, 14, https://doi.org/10.3389/fpubh.2020.00014, 2020.

1040   Marais, E. A., Jacob, D. J., Jimenez, J. L., Campuzano-Jost, P., Day, D. A. and co-authors: Aqueous-phase mechanism for secondary organic aerosol formation from isoprene: application to the southeast United States and co-benefit of SO 2 emission controls. *Atmospheric Chemistry and Physics*, *16*(3), 1603-1618, https://doi.org/10.5194/acp-16-1603-2016, 2016.

1045 Miinalainen, T., Kokkola, H., Lehtinen, K. E., and Kühn, T.: Comparing the radiative forcings of the anthropogenic aerosol emissions from Chile and Mexico. *Journal of Geophysical Research: Atmospheres*, *126*(10), https://doi.org/10.1029/2020JD033364, 2021.

Myhre, G., Samset, B. H., Schulz, M., Balkanski, Y., Bauer, S., Berntsen, T. K. and co-authors: Radiative forcing of the direct aerosol effect from AeroCom Phase II simulations. *Atmospheric Chemistry and Physics*, *13*(4), 1853-1877, https://doi.org/10.5194/acp-13-1853-2013, 2013.

1050 Nenes, A., Pandis, S. N., and Pilinis, C.: ISORROPIA: A new thermodynamic equilibrium model for multiphase multicomponent inorganic aerosols. *Aquatic geochemistry*, *4*, 123-152, https://doi.org/10.1023/A:1009604003981, 1998.

Nenes, A., Pandis, S. N., Weber, R. J., and Russell, A.: Aerosol pH and liquid water content determine when particulate matter is sensitive to ammonia and nitrate availability. *Atmospheric Chemistry and* 1055 *Physics*, *20*(5), 3249-3258, https://doi.org/10.5194/acp-20-3249-2020, 2020.

Pilinis, C. and Seinfeld, J. H.: Continued development of a general equilibrium model for inorganic multicomponent atmospheric aerosols. *Atmospheric Environment (1967)*, *21*(11), 2453-2466, https://doi.org/10.1016/0004-6981(87)90380-5, 1987.

Pope, C. A., Burnett, R. T., Turner, M. C., Cohen, A., Krewski, D. and co-authors: Lung cancer and 1060 cardiovascular disease mortality associated with ambient air pollution and cigarette smoke: shape of the exposure–response relationships. *Environmental health perspectives*, *119*(11), 1616-1621, https://doi.org/10.1289/ehp.1103639, 2011.

Pozzer, A., Jöckel, P., Sander, R., Williams, J., Ganzeveld, L., and Lelieveld, J.: The MESSy-submodel AIRSEA calculating the air-sea exchange of chemical species. *Atmospheric Chemistry and Physics*, *6*(12), 1065 5435-5444, https://doi.org/10.5194/acp-6-5435-2006, 2006.

Pringle, K. J., Tost, H., Message, S., Steil, B., Giannadaki, D. and co-authors: Description and evaluation of GMXe: a new aerosol submodel for global simulations (v1). *Geoscientific Model Development*, *3*(2), 391-412, https://doi.org/10.5194/gmd-3-391-2010, 2010.

Pringle, K. J., Tost, H., Message, S., Steil, B., Giannadaki, D. and co-authors: Corrigendum to "Description 1070 and evaluation of GMXe: a new aerosol submodel for global simulations (v1)". *Geoscientific Model Development*, *3*(2), 413-413, https://doi.org/10.5194/gmd-3-413-2010, 2010.

Putaud, J. P., Van Dingenen, R., Alastuey, A., Bauer, H., Birmili, W. and co-authors: A European aerosol phenomenology–3: Physical and chemical characteristics of particulate matter from 60 rural, urban, and kerbside sites across Europe. *Atmospheric Environment*, *44*(10), 1308-1320, 1075 https://doi.org/10.1016/j.atmosenv.2009.12.011, 2010.

Roeckner, E., Brokopf, R., Esch, M., Giorgetta, M., Hagemann, S. and co-authors: Sensitivity of simulated climate to horizontal and vertical resolution in the ECHAM5 atmosphere model. *Journal of Climate*, *19*(16), 3771-3791, https://doi.org/10.1175/JCLI3824.1, 2006.

Saiz-Lopez, A. and von Glasow, R.: Reactive halogen chemistry in the troposphere. *Chemical Society* 1080 *Reviews*, *41*(19), 6448-6472, https://doi.org/10.1039/C2CS35208G, 2012.

Sander, R., Baumgaertner, A., Cabrera-Perez, D., Frank, F., Gromov, S. and co-authors: The community atmospheric chemistry box model CAABA/MECCA-4.0. *Geoscientific model development*, *12*(4), 1365-1385, https://doi.org/10.5194/gmd-12-1365-2019, 2019.

Savoie, D. L. and Prospero, J.: Particle size distribution of nitrate and sulfate in the marine 1085 atmosphere. *Geophysical Research Letters*, *9*(10), 1207-1210, https://doi.org/10.1029/GL009i010p01207, 1982.

Saxena, P., Hudischewskyj, A. B., Seigneur, C., and Seinfeld, J. H.: A comparative study of equilibrium approaches to the chemical characterization of secondary aerosols. *Atmospheric Environment (1967)*, *20*(7), 1471-1483, https://doi.org/10.1016/0004-6981(86)90019-3, 1986.

1090 Seinfeld, J. H. and Pandis, S. N.: *Atmospheric chemistry and physics: from air pollution to climate change*. John Wiley & Sons, ISBN 1118947401, 2016.

Silva, P. J., Vawdrey, E. L., Corbett, M., and Erupe, M.: Fine particle concentrations and composition during wintertime inversions in Logan, Utah, USA. *Atmospheric Environment*, *41*(26), 5410-5422, https://doi.org/10.1016/j.atmosenv.2007.02.016, 2007.

1095 Song, S., Gao, M., Xu, W., Shao, J., Shi, G., Wang, S. and co-authors: Fine-particle pH for Beijing winter haze as inferred from different thermodynamic equilibrium models. *Atmospheric Chemistry and Physics*, *18*(10), 7423-7438, https://doi.org/10.5194/acp-18-7423-2018, 2018.

Szopa, S., Naik, V., Adhikary, B., Artaxo, P., Berntsen, T. and co-authors. 2021. Short-lived climate forcers, AGU Fall Meeting 2021, held in New Orleans, LA, 13-17 December 2021, id. U13B-06,
1100 2021AGUFM.U13B..06S, 2021.

Tang, Y. S., Flechard, C. R., Dammgen, U., Vidic, S., Djuricic, V. and co-authors: Pan-European rural monitoring network shows dominance of NH 3 gas and NH 4 NO 3 aerosol in inorganic atmospheric pollution load. *Atmospheric Chemistry and Physics*, *21*(2), 875-914, . https://doi.org/10.5194/acp-21-875-2021, 2021

1105 Tarín-Carrasco, P., Im, U., Geels, C., Palacios-Peña, L., and Jiménez-Guerrero, P.: Contribution of fine particulate matter to present and future premature mortality over Europe: A non-linear response. *Environment international*, *153*, 106517, https://doi.org/10.1016/j.envint.2021.106517, 2021.

The Acid Deposition Monitoring Network in East Asia, available at :
1110 https://monitoring.eanet.asia/document/public/index

Tost, H., Jöckel, P., Kerkweg, A., Sander, R., and Lelieveld, J.: A new comprehensive SCAVenging submodel for global atmospheric chemistry modelling. *Atmospheric Chemistry and Physics*, *6*(3), 565-574, https://doi.org/10.5194/acp-6-565-2006, 2006.

Tost, H., Jöckel, P., Kerkweg, A., Pozzer, A., Sander, R., and Lelieveld, J.: Global cloud and precipitation
1115 chemistry and wet deposition: tropospheric model simulations with ECHAM5/MESSy1. *Atmospheric Chemistry and Physics*, *7*(10), 2733-2757, https://doi.org/10.5194/acp-7-2733-2007, 2007.

Tsimpidi, A. P., Karydis, V. A., and Pandis, S. N.: Response of Inorganic Fine Particulate Matter to Emission Changes of Sulfur Dioxide and Ammonia: The Eastern United States as a Case Study, *Journal of the*
1120 *Air & Waste Management Association*, 57(12), 1489-1498, https://doi.org/10.3155/1047-3289.57.12.1489 , 2007.

Tsimpidi, A. P., Karydis, V. A., Pozzer, A., Pandis, S. N., and Lelieveld, J.: ORACLE (v1. 0): module to simulate the organic aerosol composition and evolution in the atmosphere. *Geoscientific Model Development*, *7*(6), 3153-3172, https://doi.org/10.5194/gmd-7-3153-2014, 2014.

1125 Tsimpidi, A. P., Karydis, V. A., Pozzer, A., Pandis, S. N., and Lelieveld, J.: ORACLE 2-D (v2.0): an efficient module to compute the volatility and oxygen content of organic aerosol with a global chemistry–climate model, *Geoscientific Model Development*, 11(8), 3369-3389, https://doi.org/10.5194/gmd-11-3369-2018 , 2018.

U.S. Environmental Protection Agency Clean Air Markets Division
1130 *Clean Air Status and Trends Network (CASTNET), available at :* https://www.epa.gov/castnet

van der Werf, G. R., Randerson, J. T., Giglio, L., Collatz, G. J., Mu, M. and co-authors: Global fire emissions and the contribution of deforestation, savanna, forest, agricultural, and peat fires (1997–2009). *Atmospheric chemistry and physics*, *10*(23), 11707-11735, https://doi.org/10.5194/acp-10-11707-2010, 2010.

1135 Vignati, E., Wilson, J., and Stier, P.: M7: An efficient size-resolved aerosol microphysics module for large-scale aerosol transport models. *Journal of Geophysical Research: Atmospheres*, *109*(D22), https://doi.org/10.1029/2003JD004485, 2004.

Weagle, C. L., Snider, G., Li, C., Van Donkelaar, A., Philip, S., Bissonnette, P., Burke, J., Jackson, J., Latimer, R., and Stone, E.: Global sources of fine particulate matter: interpretation of PM2. 5 chemical

1140   composition observed by SPARTAN using a global chemical transport model, *Environmental science & technology*, 52(20), 11670-11681, https://doi.org/10.1021/acs.est.8b01658, 2018.

Wexler, A. S. and Clegg, S. L.: Atmospheric aerosol models for systems including the ions H+, NH4+, Na+, SO42−, NO3−, Cl−, Br−, and H2O. *Journal of Geophysical Research: Atmospheres*, *107*(D14), ACH-14, https://doi.org/10.1029/2001JD000451, 2002.

1145 Wexler, A. S. and Seinfeld, J. H.: Second-generation inorganic aerosol model. *Atmospheric Environment. Part A. General Topics*, *25*(12), 2731-2748, https://doi.org/10.1016/0960-1686(91)90203-J, 1991.

Wolff, G. T.: On the nature of nitrate in coarse continental aerosols. *Atmospheric Environment (1967)*, *18*(5), 977-981, https://doi.org/10.1016/0004-6981(84)90073-8, 1984.

World Health Organization. Ambient (outdoor) air pollution: https://www.who.int/news-room/fact-
1150   sheets/detail/ambient-(outdoor)-air-quality-and-health, last access: 19 December 2022.

Xu, G., Zhang, Q., Yao, Y., and Zhang, X.: Changes in PM2. 5 sensitivity to NO x and NH3 emissions due to a large decrease in SO2 emissions from 2013 to 2018. *Atmospheric and Oceanic Science Letters*, *13*(3), 210-215, https://doi.org/10.1080/16742834.2020.1738009, 2020.

Yan, W., Topphoff, M., Rose, C., and Gmehling, J.: Prediction of vapor–liquid equilibria in mixed-solvent
1155   electrolyte systems using the group contribution concept. *Fluid Phase Equilibria*, *162*(1-2), 97-113, https://doi.org/10.1016/S0378-3812(99)00201-0, 1999.

Yienger, J. J. and Levy, H.: Empirical model of global soil-biogenic NOχ emissions. *Journal of Geophysical Research: Atmospheres*, *100*(D6), 11447-11464, https://doi.org/10.1029/95JD00370, 1995.

Zakoura, M. and Pandis, S. N.: Overprediction of aerosol nitrate by chemical transport models: The role of
1160   grid   resolution. *Atmospheric   Environment*, *187*,   390-400, https://doi.org/10.1016/j.atmosenv.2018.05.066, 2018.

Zuend, A., Marcolli, C., Luo, B. P., and Peter, T.: A thermodynamic model of mixed organic-inorganic aerosols to predict activity coefficients. *Atmospheric Chemistry and Physics*, *8*(16), 4559-4593, https://doi.org/10.5194/acp-8-4559-2008, 2008.

1165 Zuend, A., Marcolli, C., Booth, A. M., Lienhard, D. M., Soonsin, V., Krieger, U. K., Topping, D. O., McFiggans, G., Peter, T., and Seinfeld, J. H.: New and extended parameterization of the thermodynamic model AIOMFAC: calculation of activity coefficients for organic-inorganic mixtures containing carboxyl, hydroxyl, carbonyl, ether, ester, alkenyl, alkyl, and aromatic functional groups, *Atmospheric Chemistry and Physics*, *11*(17), 9155-9206, https://doi.org/10.5194/acp-11-9155-2011, 2011.

1170